N73-30863

NASA CONTRACTOR REPORT

NASA CR-2216

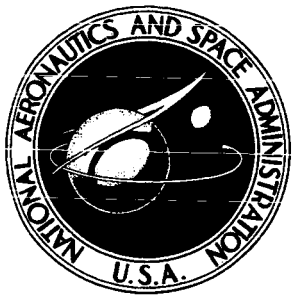

NASA CR-2216

COPY

ELASTIC BUCKLING ANALYSIS FOR COMPOSITE STIFFENED PANELS AND OTHER STRUCTURES SUBJECTED TO BIAXIAL INPLANE LOADS

by A. V. Viswanathan and M. Tamekuni

Prepared by
THE BOEING COMMERCIAL AIRPLANE COMPANY
Seattle, Wash.
for Langley Research Center

NATIONAL AERONAUTICS AND SPACE ADMINISTRATION • WASHINGTON, D. C. • SEPTEMBER 1973

1. Report No.	2. Government Accession No.	3. Recipient's Catalog No.
NASA CR-2216		

4. Title and Subtitle	5. Report Date
ELASTIC BUCKLING ANALYSIS FOR COMPOSITE STIFFENED PANELS AND OTHER STRUCTURES SUBJECTED TO BIAXIAL INPLANE LOADS	SEPTEMBER 1973
	6. Performing Organization Code
7. Author(s)	8. Performing Organization Report No.
A. V. VISWANATHAN AND M. TAMEKUNI	
9. Performing Organization Name and Address	10. Work Unit No. 501-22-01-02
THE BOEING COMMERCIAL AIRPLANE COMPANY SEATTLE, WASHINGTON	11. Contract or Grant No. NAS1-8858
	13. Type of Report and Period Covered CONTRACTOR REPORT
12. Sponsoring Agency Name and Address	14. Sponsoring Agency Code
NATIONAL AERONAUTICS AND SPACE ADMINISTRATION WASHINGTON, D. C. 20546	

15. Supplementary Notes

THIS IS A TOPICAL REPORT.

16. Abstract

AN EXACT LINEAR ANALYSIS METHOD IS PRESENTED FOR PREDICTING BUCKLING OF STRUCTURES WITH ARBITRARY UNIFORM CROSS SECTION. THE STRUCTURE IS IDEALIZED AS AN ASSEMBLAGE OF LAMINATED PLATE-STRIP ELEMENTS, CURVED AND PLANAR, AND BEAM ELEMENTS. ELEMENT EDGES NORMAL TO THE LONGITUDINAL AXES ARE ASSUMED TO BE SIMPLY SUPPORTED. ARBITRARY BOUNDARY CONDITIONS MAY BE SPECIFIED ON ANY EXTERNAL LONGITUDINAL EDGE OF PLATE-STRIP ELEMENTS. THE STRUCTURE OR SELECTED ELEMENTS MAY BE LOADED IN ANY DESIRED COMBINATION OF INPLANE TRANSVERSE COMPRESSION OR TENSION SIDE LOAD AND AXIAL COMPRESSION LOAD. THE ANALYSIS SIMULTANEOUSLY CONSIDERS ALL POSSIBLE MODES OF INSTABILITY AND IS APPLICABLE FOR THE BUCKLING OF LAMINATED COMPOSITE STRUCTURES. NUMERICAL RESULTS FROM THE ASSOCIATED COMPUTER PROGRAM "BUCLASP2" ARE PRESENTED. THE NUMERICAL RESULTS CORRELATE WELL WITH THE RESULTS OF PREVIOUS ANALYSIS METHODS.

17. Key Words (Suggested by Author(s))	18. Distribution Statement
BUCKLING OF STIFFENED PANELS LAMINATED COMPOSITE; BIAXIAL LOADING RESULTS FROM COMPUTER PROGRAM BUCLASP2 FLAT AND CURVED PLATE AND BEAM ELEMENTS	UNCLASSIFIED - UNLIMITED

19. Security Classif. (of this report)	20. Security Classif. (of this page)	21. No. of Pages	22. Price*
UNCLASSIFIED	UNCLASSIFIED	88	DOMESTIC, $3.75 FOREIGN, $6.25

*For sale by the National Technical Information Service, Springfield, Virginia 22151

CONTENTS

ELASTIC BUCKLING ANALYSIS FOR COMPOSITE STIFFENED PANELS AND OTHER STRUCTURES SUBJECTED TO BIAXIAL INPLANE LOADS

by

A. V. Viswanathan and M. Tamekuni

The Boeing Commercial Airplane Company
Seattle, Washington

1.0 SUMMARY

An exact linear analysis method is presented for predicting buckling of structures with arbitrary uniform cross section. The structure is idealized as an assemblage of laminated plate-strip elements, curved and planar, and beam elements. Element edges normal to the longitudinal axes are assumed to be simply supported. Arbitrary boundary conditions may be specified on any external longitudinal edge of plate-strip elements. The structure or selected elements may be loaded in any desired combination of inplane transverse compression or tension side load and axial compression load.

The analysis simultaneously considers all possible modes of instability and is applicable for the buckling of laminated composite structures. Numerical results from the associated computer program "BUCLASP2", Ref. 9, are presented. Predicting a previously unknown buckling mode shape for a zee-stiffened panel demonstrates the generality of this method. The results for some conceptually-advanced structural panels, Fig. 5 illustrate some applications of the curved plate-strip elements. The higher buckling load predicted for the formed zee section, using the curved element to idealize the corners, illustrates the significance of ignoring the corner radius. The results also confirm the experimentally observed superiority of bonded over riveted connections and show for the example considered, the beneficial effects of offsets between elements on buckling strength. The numerical results correlate well with the results of previous analysis methods.

2.0 SYMBOLS

a	length of the structure
A_{ij}	extensional stiffnesses i, j = 1, 2, 6 equation (A.7)
A_b	cross-sectional area of beam element
b	developed width of plate-strip element
B_{ij}	stiffnesses (i, j = 1, 2, 6) associated with coupling between bending and extension, equation (A.8)
C_1	diagonal matrix of longitudinal variables, equation (B.24)
$\overline{C}_{11}$, $\overline{C}_{12}$, $\overline{C}_{22}$	biaxial stiffness of plate-strip elements, equations (B.61) and (B.62)
d	displacement vector of elements
d_{ii}	elements of the diagonal matrix D_o, equation (C.3)
D	displacement vector of total structure, equations (B.56) to (B.58)
D_o	diagonal matrix, equation (C.1) and (C.3)
D_{ij}	bending stiffnesses (i, j = 1, 2, 6) equation (A.9)
E_{11}, E_{22}	Young's modulii of orthotropic material
f	force vector of elements
$\overline{F}_{11}$, $\overline{F}_{12}$, $\overline{F}_{22}$	biaxial flexibilities of plate-strip element, equations (B.63) and (B.64)
G_j	j^{th} Galerkin multiplier, equation (E.15)
G_{12}, G_{23}	shear modulii of orthotropic material
h_k	distance to the k^{th} lamina from the reference plane
I_p	polar moment of intertia of beam element, equation (A.21)
I_{yy}, I_{zz}	moments of inertia of beam element
J	torsion constant for beam element
k_o, k_A, k_B	diagonal matrices spring constants

k_w, k_θ, k_v, k_u	spring constants
k_{1n}, ...k_{12n}	coefficients defining displacements, equations (E.9) to (E.14)
K, K_o, K_g	total, elastic and geometric stiffness matrix, respectively, equation (B.56) and (B.57)
$\bar{K}_o$, $\bar{K}_1$, ...$\bar{K}_8$	coefficients of characteristic equation (B.7)
$\bar{K}_{uo}$, $\bar{K}_{u1}$,...$\bar{K}_{u4}$	coefficients of characteristic equation (D.6)
ℓ	number of laminas
L	unit lower triangular matrix
L_{1i}, L_{2i}, L_{3i}	displacement ratio coefficients, equations (B.9) and (D.8)
$\bar{L}_1$, $\bar{L}_2$, ...$\bar{L}_6$	linear differential operators, equation (E.4)
m	half-wave number, equation (B.3)
M_{11}, M_{12}, M_{22}	moment resultants, equation (A.6)
M_x	torque on the beam element
$\hat{M}$	moment resultant, equation (B.2)
n	circumferential wave number
N_{11}, N_{12}, N_{22}	stress resultants, equation (A.5)
$\bar{N}_{11}$, $\bar{N}_{22}$	applied inplane loads
$\hat{N}$	effective stress resultant in y-direction, equation (B.2)
p_i, p_{ui}, p_{wi}	buckling displacement parameters, equations (B.3) and (D.1) to (D.3)
P	axial load in beam element induced by buckling, equation (A.32)
P_m	minimum buckling load of the structure for a chosen m value

P_r	buckling load of plate-strip elements, when the longitudinal (x) sides are completely restrained.
P_{trial}	current trial value of the external loads in the iteration process
P_u	upper bound to the buckling load of the structure
$\bar{P}_b$	applied axial load in beam
q_y, q_z	lateral shears on the beam element equation (A.29) and (A.31)
Q_{ij}	orthotropic material constants (i, j = 1, 2, 6), equation (A.4)
Q_2, $\hat{Q}$, Q_s	effective transverse shear parallel to z-axis in plate-strip elements, equations (B.2) and (B.25)
R	reference plane radius of the curved plate-strip element
R_{11}, R_{12} ...R_{33}	elements of coefficient matrix R, equation (B.5)
s_1, s_{11}, s_{12} s_{21}, s_{22}	stiffness matrices for plate-strip elements
s_b	stiffness matrix for beam element
s_A, s_B	reduced stiffness matrices for plate-strip element, equations (B.46) and (B.49), respectively
S	stiffness matrix of total structure
t_k	thickness of k^{th} layer of a laminate
$\tilde{T}_o$, $\tilde{T}_A$, $\tilde{T}_B$, $\tilde{T}_b$	transformation matrices
$\hat{T}$	effective inplane shear in plate-strip elements, equation (B.2)
u, v, w	displacements at the reference plane of plate-strip element and at the shear center of beam element

U_s	change in strain energy
U_b, V_b, W_b	buckling displacement coefficient for beam element, equation (B.50)
U_i, V_i, W_i	buckling displacement coefficients for plate-strip element, equation (B.3)
W_e	change in potential energy of the applied loads
W_m	buckling displacement coefficients, equation (E.7)
x, y, z	orthogonal coordinates, figures (A.1) and (A.2)
X_1, X_2	matrices for plate-strip elements defined in equations (B.22) and (B.29) respectively
X_3, X_4	matrices for plate-strip element defined in equations (B.34) and (B.35) respectively.
X_5	matrix for beam element defined in equation (B.51)
y_o, z_o	plate-strip element offsets, figure 19
y_m, z_m	distances measured parallel to the y and z axes, respectively, from the shear center of the beam element to its neutral axis
Y_{1n}, Y_{2n}	buckling displacement coefficients, equation (E.7)
α, β_i	buckling displacement parameters, equations (B.3) and (B.50)
β_{1i}, β_{2i}	buckling displacement parameters, equations (D.1) to (D.4)
γ_{xy}	shearing strain
Γ	warping constant of beam element
ϵ_x, ϵ_y	normal strains
ζ	angle subtended at its center of curvature by the plate-strip element, figure 19

η, η_o, η_s	root count numbers, equation (C.2)
θ	rotation or twist
Θ_b	beam twist coefficient, equation (B.50)
κ_x, κ_y, κ_{xy}	change in curvatures
λ	proportionality factor, equation (B.57)
ν_{12}, ν_{21}	Poisson's ratio
π	total potential
σ_x, σ_y	normal stresses
σ_{xy}	shear stress
φ, φ_A, φ_B	transformation angles, equations (B.31) to (B.33)
ψ	angle between y_G axis and the chord of plate-strip element, figure 19

Subscripts

AD	quantities along the side AD of plate-strip element
b	quantities related beam element
BC	quantities along the side BC of plate-strip element
G	quantities related to global axes
i	index corresponding to characteristic roots
(j)	index for element numbers
k	layer index
n	index for number of terms
s	quantities with offset effects

A subscript preceded by a comma indicates partial differentation with respect to the subscript.

Superscripts

k	layer index
T	matrix transpose
°	quantities in the reference plane of plate-strip element
+	quantities along the side $y = +\frac{b}{2}$ of plate-strip element
-	quantities along the side $y = -\frac{b}{2}$ of plate-strip element

3.0 INTRODUCTION

Continuing efforts at increasing the strength-to-weight ratio of aerospace and missile structures have led to novel concepts in design and to use of new materials. Keeping in pace with this trend, a method is presented here for the buckling analysis of structures like stiffened panels, under biaxial loads.

A unified linear buckling analysis for flat stiffened panels under uniaxial compression is given in Ref. 1. Therein the panels are idealized as an assemblage of a series of linked flat plate-strip elements and beam elements, of uniform cross section, the individual elements extending over the full length of the panel. The edges of each element normal to the longitudinal axis are simply supported with no restriction on the axial (warping) displacements. The beam elements are used to idealize lips or beads in structural sections, or any local reinforcement, in the form of a lumped area of material. The unified buckling analysis makes no a priori assumption of the buckling mode, except that the half-wavelength of buckling is the same in all the elements of the stiffened panel. The analysis yields the lowest buckling load and the corresponding mode shape irrespective of the type of buckling. The accuracy and the generality of the method are illustrated by the results presented in Refs. 1 and 2.

In aerospace structures, panels with curved parts, Ref. 3, are often used. Figure 1 shows some typical examples. Though the curved parts can in the limit be idealized as a series of flat plate-strips, computationally it is not economical to do so. It is better to idealize them using curved plate-strip elements as in the present analysis. These circular cylindrical strip elements have constant curvature with zero Gaussian curvature. A variety of linear theory equations involving various degrees of approximations and resulting limitations are available in the literature, e.g. Refs. 4 and 5, for thin cylindrical shells. Since the present analysis which covers all modes of buckling does not restrict the range of radius-to-length ratio of the curved plate-strip elements, the proper choice of the equations becomes significant. Further, as discussed later, the stiffness matrix of the curved plate-strip elements, derived from these equations, must be symmetric. Thus, to suit the requirements of the present buckling analysis, the necessary equations and the consistent boundary conditions are developed using variational methods. These equations are based on the geometry of shell deformations given in Ref. 6. The inplane external loading is uniform and biaxial. The equations degenerate to those of the flat plate-strip element, in the limiting case of zero curvature

The curved and flat plate-strip elements are in general laminated. For each lamina, the stress-strain equations used in the analysis assume orthotropy with respect to the axes of the stiffened plate. This is exact for fiber reinforced composites when the fiber directions in each lamina are

either along the plate axis or orthogonal to it. This assumption of orthotropy is a good approximation for balanced composites with many plies. For such practical structures, this assumption reduces the analysis complexity considerably and is not considered to be unduly restrictive.

Elementary theory of bending and torsion is used for the beam elements. The external loading on them is uniform and axial. The physical properties of laminated beams are calculated in an approximate manner.

The analysis considers offsets between elements and effects of arbitrary elastic restraints along any external longitudinal side (i.e., not connected to other elements) of the flat or curved plate-strip elements.

In Ref. 1, the buckling criteria is derived in determinantal form by enforcing separately the compatibility of buckling displacements and the equilibrium of the corresponding forces along the inter-element junction lines, expressed in terms of the displacement amplitude coefficients. The resulting buckling determinant is unsymmetric and the method of repetitive determinant evaluation, incrementing the load in steps, is the only recourse to obtain the buckling load. Unless the load is incremented in sufficiently small steps, one is apt to miss the lowest buckling load, and the method will unknowingly yield the buckling load corresponding to a higher mode. Thus, the major drawbacks of the method are the difficulty in defining the magnitude of the load step for a particular problem, and the considerable increase in computation time associated with the reduction in step size. These are overcome in the present analysis by reformulating the buckling criteria of Ref. 1. For each element making up the stiffened panel, a symmetric stiffness matrix is derived relating the forces to the corresponding displacements along its inter-element junction lines. The symmetric overall stiffness matrix of the stiffened panel, which is obtained by suitably merging the individual element stiffness matrices, corresponds to the unsymmetric "buckling determinant" of Ref. 1, and is considerably smaller in size. The symmetry, enables the use of the algorithm described in Ref. 7, to isolate with certainty and in relatively fewer load iterations, the lowest buckling load. A primary requirement of this algorithm is an upper bound for the panel buckling load, resulting from completely restraining all the inter-element junction lines. Such a bounding value is obtained here, by applying the Galerkin method, Ref. 8, for each strip element.

The elements of the stiffness matrix are transcendental functions of the external loadings and the half-wave length of buckling. For each assumed half-wave length (or integer number of longitudinal half-waves in the stiffened panel), the lowest level of applied loads at which the determinant of the overall stiffness matrix vanishes is the buckling load. The lowest of these loads is then the critical load for the panel. The buckling mode shape is obtained from the eigenvector solution of the stiffness matrix at the critical load. Detailed discussions on the usefulness of the buckling mode shape plots, in achieving efficient design of stiffened plates is discussed and illustrated in Refs. 1 and 2.

The buckling analysis is applicable to any structure of uniform cross section which can be idealized as an assemblage of the different types of elements described earlier. The intersecting angle between elements is arbitrary. The structure may be loaded in any desired combination of transverse load in the plane of selected plate-strip elements and axial load. The stiffened panel, flat and curved, under biaxial inplane loading is a particular case of such structure. In these panels, it is reasonable to assume that the side load normal to the axis of the stiffeners is carried entirely by the plate-strip elements covering the skin.

The basic assumptions governing the analysis are:

(a) The material is linearly elastic.

(b) Each lamina is orthotropic.

(c) The Kirchhoff-Love hypothesis is used for the deformation across the thickness.

(d) Effects of pre-buckling deformations are ignored. Thus, at buckling each plate-strip element, whether flat or curved, is in general, in a state of uniform biaxial inplane loading. Each beam element is under uniform axial load.

(e) The edges of each element along $x = 0$ and $x = a$, Figures 16 and 17, are simply supported in the classical sense.

The computer program "BUCLASP2", Ref. 9, based on the present analysis is written for the CDC 6600 computer.

4.0 RESULTS

The details of the buckling analysis are given in the Appendices. The analysis is general and has the capability to analyze laminated composite structures. For these structures, lack of other published data makes it very difficult to correlate in detail the numerical results. Thus, the results presented below while verifying the analysis, do not relfect its full capabilities.

The results are categorized into (a) "prior results", referring to the results quoted in Refs. 1 and 2, and (b) further results.

All results were obtained using the associated computer program "BUCLASP2" Ref. 9.

4.1 Prior Results

Refs. 1 and 2 give the buckling results for a variety of structures assembled from flat plate-strip elements and beam elements only. The computer program "BUCLASP2" yielded identical results, thus confirming the very good correlations obtained earlier for structures of this type. Interested readers are referred to the above references.

4.2 Further Results

The results given below are mainly for structures incorporating circular arc components idealized as curved plate-strip elements.

(i) Isotropic and fiber reinforced cylindrical shells.--In Appendix A, for the reasons discussed therein, the basic equations for the curved plate-strip element are derived from the variational principles. Figure 2 shows the results from Donnell's equations superposed on the curves of Figure 11.4 of Ref. 10. The well-known deficiency of Donnell's equations for small circumferential wave numbers is apparent. The results from the present analysis shown as discrete points on the curves, show that the equations of Appendix A yield the desired Euler mode results for long cylinders and local buckling results for short cylinders. The cylinders are idealized in the present analysis as an assemblage of at least two curved plate-strip elements, each covering one half of the cylinder (180 degrees).

The geometry and the material properties of a series of aluminum cylinders overwound with boron-epoxy layers are shown in Figure 3. The cylinders are all identical except for the difference in wrap angle of the boron filaments. The data is taken from Ref. 11, wherein the buckling of these cylinders under axial compression is studied. For the boron-epoxy layers the modulus E_{11} is in the direction of the cylinder axis and E_{22} in the perpendicular direction.

Figure 3 also shows the results from Ref. 11 based on Donnell's theory and the results from the present analysis. For the latter, two sets of results are quoted. The first set is the result of suppressing the underlined terms in equations (A.1) and (A.13) to (A.22). This, in effect, reduces these equations to those of Donnell's theory. The second set is the result of retaining all the terms in the above equations. The circumferential wave number from the present analysis corresponding to each buckling load is determined from the mode shape plot. The first of these sets of results are almost identical to those from Ref. 11. The second set of results from the "complete" analysis of the present method are generally lower, the difference being 3 to 4% for the higher fiber angles. It is noticed that for the fiber angle of 90° the latter result has the minimum buckling load at $m = 1$ compared to $m = 2$ for Donnell's theory. Though not quoted here, the results from the present "complete" analysis correlated excellently with the results obtained from Timoshenko's cylindrical shell equations, Ref. 10

(ii) Advanced structural panels --Figure 4 shows some of the panels currently being developed under NASA Contract NAS1-10749, "Design and Testing of Advanced Structural Panels."[1] An isolated portion of each of panels 1 to 5 and the whole of panel 6, with the indicated boundary conditions, were analyzed. In Figure 5 the results of the present analysis are presented as the plot of buckling load versus half-wavelength of buckling ($\frac{a}{m}$). Also shown are the buckling mode shapes for selected half-wave lengths. Results for panels 1 to 5 obtained using the computer program "BOSOR3", Ref. 12, based on the analysis of Ref. 13, are also shown for comparison.

(iii) Laminated curved plates under biaxial loads.--A two-layered plate, shown in Figure 6, with all edges simply supported is chosen to verify the results of the present analysis for biaxially loaded plates. The above boundary conditions enable a closed form solution to be obtained by applying the displacement functions used in Ref. 10 for "axial compression of curved sheet panels." The results from such a solution is given in Figure 7, in the form of an interaction curve. The results of the present analysis are superposed on this curve. The above correlation procedure is adopted in the

---

[1] Work performed by The Boeing Company, Aerospace Group, P. O. Box 3999, Seattle, Washington 98124.

absence of published results for such biaxially loaded plates. The present analysis can be readily used to generate interaction curves similar to Figure 7, not only for plates with arbitrary conditions along sides AB and BC, but also for structures like stiffened panels.

(iv) Curved stiffened panel under biaxial loads.--The arbitrarily chosen panel shown in Figure 8 is idealized using the curved plate-strip elements for the skin, flat plate-strip elements for the integral stiffeners and beam elements for the local reinforcement on the skin between stiffeners. Keeping the transverse inplane load $\bar{N}_{22}$ constant for this example, the buckling analysis yields the critical value of the axial load and the corresponding strain. The results together with the buckling mode shape are shown in Figure 9. From such data, interaction curves for buckling of biaxially loaded panels can be readily derived.

(v) Panel with zee stiffeners. --Figure 10 shows a panel with zee stiffeners. The results of the present buckling analysis reveals an interesting and hitherto unknown mode shape. The buckling mode has a characteristic half-wavelength across the panel width, involving multi-stiffeners. Classical buckling analyses run the risk of missing such modes because of their simplified assumptions regarding mode shapes.

5.0 DISCUSSION

Some observations of particular interest resulting from the preliminary numerical study of the buckling analysis are discussed here. These also serve to bring out some of the features of the analysis.

5.1 Buckling of Formed Sections

Section 4 illustrates the general applications of the curved plate-strip elements. The present example considers the effect of using curved plate-strip elements to idealize the corners of formed structural sections. Figure 11 shows a formed titanium zee section. Also shown are two different ways of idealizing this structure. The first idealization uses flat plate-strip elements only in the manner of Ref. 14. Each element extends to the intersection of the flat parts of the zee section. The second idealization uses the curved plate-strip elements for the corners, intuitively a better representation of the formed zee section.

The results of the local buckling study under uniaxial compressive loads are shown in Figure 12. It is seen that the use of curved plate-strip elements to model the corners, yields a 19% increase in minimum buckling stress. This results from the higher stiffness of the curved corners in comparison to the first idealization using only flat plate-strip elements. In either idealizations the minimum buckling stress occurs at the same m value of three and the buckling mode shapes are seen to be similar.

5.2 Effects of Offsets

The analysis developed considers the effect of offsets between elements. Such effects, though sometimes not included, Ref. 14, can be significant as seen from the example given here. Figure 13 shows a hat-stiffened titanium panel locally reinforced with boron fiber composite. The idealization of the panel is shown by the line through the mid-plane of each plate-strip element and clearly defines the offsets where present. Results of the buckling analysis, taking into account the offsets and also ignoring them, are given in the same figure. They show that for this particular example the offsets increase the buckling load by approximately 15%. The mode shape, though not given here, corresponded to long panel Euler buckling. Thus, the observed increase in buckling load results from higher effective moment of inertia of the panel when offsets are considered.

5.3 Bonded and Riveted Connections

In structures such as stiffened panels, reported tests, Ref. 15, have indicated marked influence of stiffener attachment method on the buckling load. In the present analysis, it is possible to differentiate between bonded and riveted connections by the modelling technique given in Ref. 2.

Figure 14 shows a zee stiffened panel. The bonded and riveted modelling are shown by lines drawn through the mid-plane of each plate-strip element. The rivet is assumed to be at the midpoint of the attached flange. The analytical results shown indicate that for this example the bonding increases the buckling load by 22.5%. Test results of Ref. 15 show the observed increase in buckling load to be 17% for zee stiffened panels. The riveted modelling is only an approximation to the discrete rivets since it results in a continuous, rigid connection along the rivet line. A somewhat similar modelling has been successfully demonstrated in Ref. 16. The riveted modelling used here does not restrain the displacements of the heel of the stiffener relative to the skin. A better modelling might be to introduce an additional node in the skin inter-connected to the node at the heel of the stiffener.

5.4 Typical Problems with Coincident Roots

The phenomenon of coincident roots and its significance are discussed in Appendix C. This phenomenon occurs in the example of the long, square tube and the thin-walled cylinder shown in Figure 15. The initial idealizations used for these examples are also shown.

As stated in Appendix C, at buckling η in equation (C.2) changes from zero to one. However, in spite of pursuing the load iteration to the single precision accuracy of the CDC 6600 computer, it was possible to isolate only a zero to two change in the η value. The results show that the corresponding buckling load is in good agreement with the classical solutions. The zero to two change in η value is explained by the fact that these structures have orthogonal buckling modes with coincident buckling loads as shown in Figure 15.d. Normally, it will not be necessary to pursue this phenomenon futher. If for some reason it is essential to study the orthogonal modes, this can be easily done by the modelling procedure discussed below. This avoids recourse to special numerical techniques available for such cases, Refs. 17 and 18.

The method aims at separating the coincident buckling loads within engineering accuracy by introducing a very small "error" in the modelling, as shown for the square tube. The results indicate that this minute "kink" in the geometry is of no engineering significance. However, it avoids the coincident buckling loads by making them distinct as seen from the change in η value. It is possible that a "kink" smaller than that shown would have sufficed. This conclusion is drawn from the procedure followed for the

thin walled cylinder. In this case for the "second" idealization the nodal data defining the extremities of each element were calculated using the standard four-figure trigonometrical table. The limited accuracy of this is sufficient to introduce "kinks" at the nodes, thereby enabling the coincident buckling loads to be separated. The corresponding buckling modes are readily obtained.

6.0 CONCLUDING REMARKS

An exact elastic buckling analysis within the limitations of the linear theory, applicable to any structure of arbitrary uniform cross section, has been presented. The structure is idealized as an assemblage of laminated curved plate-strip elements, laminated flat plate-strip elements and beam elements, each element extending the entire length of the structure. The idealization permits differentiating between bonded and riveted connections. The analysis considers the effect of offsets between elements. The structure may be loaded in any desired combination of transverse side load (in the plane of selected plate-strip elements) and axial load. Stiffened panels, flat and curved, under biaxial inplane loading are typical of such structures.

The theory is general and no assumption is made regarding the buckling mode. The structure is free to take the buckled shape corresponding to minimum energy conditions consistent with prescribed constraints along any external side of plate-strip elements. The eigenvector solution is used to determine the buckled mode shape. The capability of simultaneously considering all buckling modes, coupled with the ability to predict buckling of laminated composite structures, represents a significant advance in the state-of-the-art of buckling analysis.

Numerical results correlated well with the results of previous analysis methods for those cases where the latter are applicable. An interesting and previously unknown buckling mode shape for zee stiffened panels has been presented. This result is an indication of the above mentioned generality of the theory.

The buckle mode shape plot resulting from the eigenvector solution, is a valuable tool to design efficient buckling critical structures. Correlation for biaxially loaded stiffened panels, including panels using laminated composites, is desirable. There is a dearth of published test data for such structures.

APPENDIX A
BASIC EQUATIONS

This appendix summarizes the basic equations used later in Appendix B for the buckling analysis. Some of these equations, though readily available in the literature, are repeated here for easy reference. Since the buckling analysis of Appendix B covers all possible modes of buckling, particular care is exercised in the choice of these equations. This is particularly true in regard to the laminated curved plate equations. The widely used Donnell-type approximations have known limitations, Refs. 4 and 5. For example, these equations do not yield the Euler loads for long cylinders. Further, as will be seen later, the present linear buckling analysis is based on the stiffness matrix formulation, derived from the basic equations. The necessary symmetry condition of these matrices is dependent on the terms retained in the equations, as discussed in Ref. 19. For these reasons, the equations for the laminated curved plate are derived below from variational principles.

A.1 Laminated Curved and Flat Plates

The equations developed here are for the laminated curved plate. They degenerate to those of the laminated flat plate when the curvature becomes zero (infinite radius).

Figure 16 shows the geometry and sign conventions for the curved laminate. The x, y and z axes are assumed coincident with the fiber axes 1, 2 and 3. The mid-plane of the laminate is chosen as the reference plane. The strains and curvature changes in this plane, in terms of its displacements u, v and w are, Ref. 6:

$$\begin{aligned} \varepsilon_x^\circ &= u_{,x} \\ \varepsilon_y^\circ &= v_{,y} - \frac{w}{R} \\ \gamma_{xy}^\circ &= u_{,y} + v_{,x} \\ \kappa_x^\circ &= - w_{,xx} \end{aligned} \qquad (4.1)$$

$$\kappa_y^\circ = -w_{,yy} - \underline{\frac{1}{R} v_{,y}}$$

$$\kappa_{xy}^\circ = -2 w_{,xy} - \underline{\frac{2}{R} v_{,x}} \qquad \text{(A.1)}$$

The radius R is measured from the reference plane to the center of curvature and is positive when in the positive direction of the z-axis, as in Figure 16. Equation (A.1) reduces to the Donnell- type assumptions when the underlined terms are dropped.

The strains in any plane at distance z from the reference plane are by the Kirchhoff-Love hypothesis:

$$\begin{Bmatrix} \varepsilon_x \\ \varepsilon_y \\ \gamma_{xy} \end{Bmatrix} = \begin{Bmatrix} \varepsilon_x^\circ \\ \varepsilon_y^\circ \\ \gamma_{xy}^\circ \end{Bmatrix} + z \begin{Bmatrix} \kappa_x^\circ \\ \kappa_y^\circ \\ \kappa_{xy}^\circ \end{Bmatrix} \qquad \text{(A.2)}$$

The stress-strain equations for an orthotropic lamina are, Ref. 20:

$$\begin{Bmatrix} \sigma_x^k \\ \sigma_y^k \\ \sigma_{xy}^k \end{Bmatrix} = \begin{bmatrix} Q_{11}^k & Q_{12}^k & 0 \\ Q_{12}^k & Q_{22}^k & 0 \\ 0 & 0 & Q_{66}^k \end{bmatrix} \begin{Bmatrix} \varepsilon_x \\ \varepsilon_y \\ \gamma_{xy} \end{Bmatrix} \qquad \text{(A.3)}$$

where the superscript k identifies the lamina number and

$$Q_{11}^k = E_{11}/(1-\nu_{21}\nu_{12})$$

$$Q_{22}^k = E_{22}/(1-\nu_{21}\nu_{12}) \qquad \text{(A.4)}$$

$$Q_{12}^k = \nu_{21}E_{11}/(1-\nu_{21}\nu_{12}) = \nu_{12} E_{22}/(1-\nu_{21}\nu_{12})$$

$$Q_{66}^k = G_{12}$$

Combining equations (A.1) to (A.3) and integrating over the thickness of the laminate, the stress resultants N and the moment resultants M in the reference plane are:

$$\begin{Bmatrix} N_{11} \\ N_{22} \\ N_{12} \end{Bmatrix} = \begin{bmatrix} A_{11} & A_{12} & 0 \\ A_{12} & A_{22} & 0 \\ 0 & 0 & A_{66} \end{bmatrix} \begin{Bmatrix} \varepsilon_x^\circ \\ \varepsilon_y^\circ \\ \gamma_{xy}^\circ \end{Bmatrix} + \begin{bmatrix} B_{11} & B_{12} & 0 \\ B_{12} & B_{22} & 0 \\ 0 & 0 & B_{66} \end{bmatrix} \begin{Bmatrix} \kappa_x^\circ \\ \kappa_y^\circ \\ \kappa_{xy}^\circ \end{Bmatrix} \quad (A.5)$$

$$\begin{Bmatrix} M_{11} \\ M_{22} \\ M_{12} \end{Bmatrix} = \begin{bmatrix} B_{11} & B_{12} & 0 \\ B_{12} & B_{22} & 0 \\ 0 & 0 & B_{66} \end{bmatrix} \begin{Bmatrix} \varepsilon_x^\circ \\ \varepsilon_y^\circ \\ \gamma_{xy}^\circ \end{Bmatrix} + \begin{bmatrix} D_{11} & D_{12} & 0 \\ D_{12} & D_{22} & 0 \\ 0 & 0 & D_{66} \end{bmatrix} \begin{Bmatrix} \kappa_x^\circ \\ \kappa_y^\circ \\ \kappa_{xy}^\circ \end{Bmatrix} \quad (A.6)$$

The A, B and D coefficient matrices define the overall extensional, coupling and bending stiffnesses, respectively, of the laminate, in relation to the chosen reference plane (here, the mid-plane). The elements of these matrices are, Ref. 20:

$$A_{ij} = \sum_{k=1}^{\ell} Q_{ij}{}^k \cdot t_k \quad (A.7)$$

$$B_{ij} = \frac{1}{2} \sum_{k=1}^{\ell} Q_{ij}{}^k (h_{k+1} + h_k) \cdot t_k \quad (A.8)$$

$$D_{ij} = \frac{1}{3} \sum_{k=1}^{\ell} Q_{ij}{}^k (h_{k+1}^2 + h_{k+1} \cdot h_k + h_k^2) \, t_k \quad (A.9)$$

$(i, j = 1, 2, 6)$

where h_k and h_{k+1} are the distances to the upper and lower surfaces, respectively, of the kth lamina. When the orthotropic axes of any lamina differs from the laminate axes, appropriate transformed values of $Q_{ij}{}^k$ are to be used in equations (A.7) to (A.9). The details are given in Ref. 20. This causes the A, B, and D matrices in equations (A.5) and (A.6) to be fully populated, by the presence of subscript '16' and '26' elements. In practical structures these elements are of relatively small magnitude and may be ignored. This simplification, while considerably reducing the complexity of the analysis, is not thought to be unduly restrictive.

The total change in potential, π, of the laminated plate is:

$$\pi = U_s + W_e \tag{A.10}$$

where, the change in strain energy is

$$U_s = \frac{1}{2}\int_0^a\int_0^b (N_{11}\overset{\circ}{\epsilon}_x + N_{22}\overset{\circ}{\epsilon}_y + N_{12}\overset{\circ}{\gamma}_{xy} + M_{11}\overset{\circ}{\kappa}_x + M_{22}\overset{\circ}{\kappa}_y + M_{12}\overset{\circ}{\kappa}_{xy})\,dxdy \tag{A.11}$$

and the change in the potential energy of the biaxial loads $\bar{N}_{11}$ and $\bar{N}_{22}$ causing buckling is

$$W_e = -\int_0^a\int_0^b N_{11}[u_{,x} + \tfrac{1}{2}(u_{,x}^2 + v_{,x}^2 + w_{,x}^2)]\,dxdy$$

$$-\int_0^a\int_0^b \bar{N}_{22}\left[(v_{,y} - \frac{w}{R}) + \frac{1}{2}\left\{(v_{,y} - \frac{w}{R})^2 + (w_{,y} + \frac{v}{R})^2 + u_{,y}^2\right\}\right]dxdy \tag{A.12}$$

The above expression for W_e reflects the possibility of significant inplane buckling displacements in any of the strip elements making up the panel. Though the effect of the terms $\int\int \bar{N}_{11}\, u_{,x}^2\, dx\, dy$ and $\int\int \bar{N}_{22}\, u_{,y}^2\, dx\, dy$ are negligible, they are retained, as observed in Ref. 19, to ensure the symmetry of the stiffness matrix for the laminated plate-strips, derived in Appendix B.

The "stability equations" of the biaxially loaded laminated plate-strip are derived here using variational principles, in a manner similar to that in Refs. 21 and 22. Effects of the pre-buckling deformations are ignored. The resulting equations are:

$$N_{11,x} + N_{12,y} - \underline{\bar{N}_{11}\, u_{,xx}} - \underline{\bar{N}_{22}\, u_{,yy}} = 0 \tag{A.13}$$

$$N_{22,y} + N_{12,x} - \underline{\frac{1}{R}\,(M_{22,y} + 2\,M_{12,x})} - \underline{\bar{N}_{11}\, v_{,xx}}$$

$$\underline{- \bar{N}_{22}\,(v_{,yy} - \frac{2}{R}\,w_{,y} - \frac{1}{R^2}\,v)} = 0 \tag{A.14}$$

$$M_{11,xx} + M_{22,yy} + 2M_{12,xy} + \frac{1}{R} N_{22} - \bar{N}_{11} w_{,xx}$$
$$-\bar{N}_{22} \left(\underline{\frac{2}{R} v_{,y}} + w_{,yy} - \underline{\frac{1}{R^2} w}\right) = 0 \qquad \text{(A.15)}$$

The variational procedure also yields consistent boundary conditions. These are, along any side of the plate-strip y = constant:

$$w = 0 \text{ or } M_{22,y} + 2M_{12,x} - \bar{N}_{22} \left(\underline{\frac{v}{R}} + w_{,y}\right) = 0 \qquad \text{(A.16)}$$

$$\left(w_{,y} + \underline{\frac{v}{R}}\right) = 0 \text{ or } M_{22} = 0 \qquad \text{(A.17)}$$

$$v = 0 \text{ or } N_{22} - \underline{\bar{N}_{22} \left(v_{,y} - \frac{w}{R}\right)} = 0 \qquad \text{(A.18)}$$

$$u = 0 \text{ or } N_{12} - \underline{\bar{N}_{22} u_{,y}} = 0 \qquad \text{(A.19)}$$

and along any edge x = constant:

$$w = 0 \text{ or } M_{11,x} + 2M_{12,y} - \bar{N}_{11} w_{,x} = 0 \qquad \text{(A.20)}$$

$$w_{,x} = 0 \text{ or } M_{11} = 0 \qquad \text{(A.21)}$$

$$v = 0 \text{ or } N_{12} - \underline{\bar{N}_{11} v_{,x}} = 0 \qquad \text{(A.22)}$$

$$u = 0 \text{ or } N_{11} - \underline{\bar{N}_{11} u_{,x}} = 0 \qquad \text{(A.23)}$$

Equations (A.13) to (A.23) reduce to Donnell-type equations for thin cylindrical shells, on dropping the underlined terms.

A.2 Laminated Beams

Concentrated local reinforcements, like beads or lips in stiffeners, corner fillets in extruded sections, any beam type boron reinforcements, etc., are idealized in the buckling analysis as beam elements. In all cases, the basic quantities involved are the gross beam properties of the element. Approximate equations to evaluate these properties, for the more common beam types, namely, the laminated rectangular and the laminated circular beam elements, are given here. Figure 17 shows the geometry and sign conventions. C is the point of intersection of the neutral axis and the beam cross section. Thus, for a uniform axial strain the corresponding resultant load passes through C. O is the shear center. A complex analysis, beyond the scope of the present panel buckling analysis, is

necessary to locate the shear center of the laminated rectangular beam. Considering the envisaged applications of the beam type elements in panels, negligible error will result in assuming that the shear center O of the laminated rectangular beam coincides with the geometric center. This is, however, exact for the laminated circular beam. Any beam element is idealized as a line in the longitudinal (x) direction through its shear center O.

The basic material properties involved are the individual lamina constants, E_{11}^{k} and G_{23}^{k} for the k^{th} lamina. The gross beam properties $E_{11}I_{yy}$, $E_{11}I_{zz}$, and $E_{11}A_b$ are calculated from

$$E_{11}\,F = \sum_{k=1}^{\ell} E_{11}^{k}\,F^{k} \tag{A.24}$$

where F denotes I_{yy}, I_{zz} or A_b. The moments of inertia I_{yy}^{k} and I_{zz}^{k} of the k^{th} lamina, are about the beam principal axes.

Also, $$\bar{\sigma}\,I_p = \sum_{k=1}^{\ell} \bar{\sigma}^{k}\,I_p^{k} \tag{A.25}$$

Where $\bar{\sigma}^{k}$ is the compressive stress in the k^{th} lamina due to the external axial load $\bar{P}_b$, the axial strain being the same in all laminas. The polar moment of inertia I_p^{k} is about the shear center, O.

The overall torsional property $G_{23}J$ of the laminated circular beam element is

$$G_{23}J = \sum_{k=1}^{\ell} G_{23}^{k}\,J^{k} \tag{A.26}$$

This equation is not suitable for the laminated rectangular beam element, since, each lamina deforms with a different eccentricity to the shear center of the overall beam section. In the absence of an exact expression, the following approximate equation is used:

$$G_{23}J = \left(\frac{\sum_{k=1}^{\ell} G_{23}^{k}\,A_b^{k}}{\sum_{k=1}^{\ell} A_b^{k}} \right) J_0 \tag{A.27}$$

Similarly,

$$E_{11}\,\Gamma = \left(\frac{\sum_{k=1}^{\ell} E_{11}{}^{k}\, A_b{}^{k}}{\sum_{k=1}^{\ell} A_b{}^{k}} \right) \Gamma_0 \qquad (A.28)$$

J_0 and Γ_0 are the St. Venant torsion constant and the warping constant, respectively, based on the overall section geometry of the laminated rectangular beam.

Equations for the various physical properties involved in equations (A.24) to (A.28), are to be found in Refs. 23, 24 and 25.

Using the theory of torsion and flexure, Ref. 10, the equations for the beam element under axial compressive load $\overline{P}_b$ are:

$$q_z = E_{11}\, I_{yy} \frac{d^4w}{dx^4} + \overline{P}_b \frac{d^2w}{dx^2} + \overline{P}_b y_m \frac{d^2\theta}{dx^2} \qquad (A.29)$$

$$\frac{dM_x}{dx} = E_{11}\, \Gamma \frac{d^4\theta}{dx^4} + (\bar{\sigma} I_p - G_{23} J) \frac{d^2\theta}{dx^2} + \overline{P}_b y_m \frac{d^2w}{dx^2} - \overline{P}_b z_m \frac{d^2v}{dx^2} \qquad (A.30)$$

$$q_y = E_{11}\, I_{zz} \frac{d^4v}{dx^4} + \overline{P}_b \frac{d^2v}{dx^2} - \overline{P}_b z_m \frac{d^2\theta}{dx^2} \qquad (A.31)$$

$$\frac{dP}{dx} = - E_{11}\, A_b \frac{d^2u}{dx^2} \qquad (A.32)$$

y_m and z_m are the distances measured parallel to the principal axes y and z, respectively, from the shear center O to the neutral axis C of the beam element. The distances are positive in the positive directions of the axis. The displacements u, v and w and the twist θ are positive in the directions shown in figure 17.

APPENDIX B

BUCKLING ANALYSIS

The equations derived in Appendix A are now used in developing a buckling analysis applicable to any structure of uniform cross section which can be readily assembled from the element types discussed earlier. The intersecting angle between elements is arbitrary. Simply supported conditions with no restriction on the axial (warping) displacements u, are assumed along the edges $x = 0$ and $x = a$ of each element, (figures 16 and 17), so that the variables in the equations can be separated. It is possible to specify arbitrary elastic restraint conditions along any external longitudinal side (y = constant) of flat or curved plate-strip elements.

Effects of pre-buckling deformations and any initial imperfections are ignored. Thus, at buckling each plate-strip element, whether flat or curved, is in a state of uniform biaxial loading of $\bar{N}_{11}$ and $\bar{N}_{22}$. The beam elements are in a state of uniform compression corresponding to $\bar{P}_b$. These element loadings determined from considerations of strain compatibility between elements in general, vary from element to element. Typical application of the biaxial loading case is to stiffened panels. For such structures the analysis assumes that the inplane loading normal to the stiffener axis is carried entirely by the plate-strip elements corresponding to the skin.

The structure is assumed to buckle into integer number of half-waves in the longitudinal (x) direction, the number being the same in all elements. Laterally, the structure is free to take the buckled shape corresponding to minimum energy conditions consistent with the constraints along any external side. The buckling load is defined as the lowest load level that causes any plate element to initiate a buckling deformation before others do (local mode) or causes several elements to have simultaneous deformation (general mode).

The chosen buckling displacement functions for each element type represent an exact solution. For the plate-strip elements, these functions are substituted in equations (A.13) to (A.15), resulting in a characteristic polynomial equation. At any chosen load level, the roots of this polynomial are used in obtaining the stiffness matrix of the element, relating the buckling displacements and the corresponding forces along the inter-element junction lines. A corresponding stiffness matrix is derived for the beam element. The element stiffness matrices are merged to form the stiffness matrix of the total structure. The buckling load is evaluated from this total stiffness matrix by an iteration procedure based on an algorithm analogous to the use of Sturm sequence property, Ref. 17. The algorithm uses an upper-bound to the buckling load of the structure obtained by considering all inter-element junction lines to be completely restrained. The buckling loads for a series of buckling half-wave numbers in the longitudinal (x) direction are investigated. The lowest of these loads is the critical load for the structure. The corresponding mode shape is then obtained from the eigenvector solution.

B.1 Stiffness of Curved and Flat Plate-Strip Elements

Equations are now derived for the stiffnesses relating the displacements due to buckling and the corresponding forces along the sides $y = \pm \frac{b}{2}$ of the laminated curved plate-strip element, under biaxial loads $\bar{N}_{11}$ and $\bar{N}_{22}$. These equations degenerate to those of the laminated flat plate-strip element, in the limit of the curvature becoming zero (infinite radius).

The displacements involved are:

$$w, \ (\theta = w_{,y} + \frac{v}{R}), \ v \text{ and } u. \tag{B.1}$$

The corresponding forces are:

$$\hat{Q} = Q_2 - \bar{N}_{22} \ (w_{,y} + \frac{v}{R})$$

$$(\text{where } Q_2 = M_{22,y} + 2M_{12,x})$$

$$\hat{M} = M_{22} \tag{B.2}$$

$$\hat{N} = N_{22} - \bar{N}_{22} \ (v_{,y} - \frac{w}{R})$$

$$\text{and } \hat{T} = N_{12} - \bar{N}_{22} \ u_{,y}$$

respectively, as seen from equations (A.16) to (A.19).

Choosing the mid-plane as the reference plane, the assumed buckling displacement functions are:

$$w = \sum_{i=1}^{8} W_i \ e^{\beta_i} \sin \alpha$$

$$\alpha = m\pi x/a$$

$$v = \sum_{i=1}^{8} V_i \ e^{\beta_i} \sin \alpha \tag{B.3}$$

$$\beta_i = p_i \pi y/a$$

$$u = \sum_{i=1}^{8} U_i \ e^{\beta_i} \cos \alpha$$

p_i $(i = 1, 2, \ldots 8)$ are the roots of the characteristic equation, discussed later.

The above functions are chosen to satisfy ab initio the simply supported boundary conditions defined by:

$$w = M_{11} = v = (N_{11} - \bar{N}_{11}\, u_{,x}) = 0 \qquad (B.4)$$

along the edges $x = 0$ and $x = a$. At any particular level of external loads $\bar{N}_{11}$ and $\bar{N}_{22}$, on substituting a typical term of the displacement functions and equations (A.1), (A.5) and (A.6) into the curved plate equations (A.13) to (A.15), yields:

$$\begin{bmatrix} R_{11} & R_{12} & \pi R_{13} \\ R_{21} & R_{22} & \pi R_{23} \\ R_{31} & R_{32} & \pi R_{33} \end{bmatrix} \begin{Bmatrix} U_i \\ V_i \\ W_i \end{Bmatrix} = 0 \qquad (B.5)$$

where

$$R_{11} = - A_{11} \left(\frac{m}{a}\right)^2 + A_{66} \left(\frac{p_i}{a}\right)^2 + \bar{N}_{11} \left(\frac{m}{a}\right)^2 - \bar{N}_{22} \left(\frac{p_i}{a}\right)^2$$

$$R_{12} = (A_{12}+A_{66}) \cdot \left(\frac{m}{a}\right)\left(\frac{p_i}{a}\right) - \frac{1}{R} (B_{12}+2B_{66})\left(\frac{p_i}{a}\right) \left(\frac{m}{a}\right)$$

$$R_{13} = B_{11}\left(\frac{m}{a}\right)^3 - (B_{12}+2B_{66}) \left(\frac{m}{a}\right) \left(\frac{p_i}{a}\right)^2 - \frac{A_{12}}{\pi^2 R} \left(\frac{m}{a}\right)$$

$$R_{21} = - R_{12}$$

$$R_{22} = A_{22} \left(\frac{p_i}{a}\right)^2 - A_{66}\left(\frac{m}{a}\right)^2 + \frac{4}{R} \left(B_{66} - \frac{D_{66}}{R}\right)\left(\frac{m}{a}\right)^2 + \frac{1}{R} \left(\frac{D_{22}}{R} - 2B_{22}\right)\left(\frac{p_i}{a}\right)^2$$

$$+ \bar{N}_{11} \left(\frac{m}{a}\right)^2 - \bar{N}_{22} \left\{ \left(\frac{p_i}{a}\right)^2 - \frac{1}{\pi^2 R^2} \right\} \qquad (B.6)$$

$$R_{23} = (B_{12}+2B_{66}) \left(\frac{m}{a}\right)^2 \left(\frac{p_i}{a}\right) - B_{22} \left(\frac{p_i}{a}\right)^3 - \frac{A_{22}}{\pi^2 R} \left(\frac{p_i}{a}\right) + \frac{B_{22}}{\pi^2 R^2} \left(\frac{p_i}{a}\right)$$

$$+ \frac{D_{22}}{R} \left(\frac{p_i}{a}\right)^3 - \frac{1}{R} (D_{12}+4D_{66}) \left(\frac{p_i}{a}\right) \left(\frac{m}{a}\right)^2 + \bar{N}_{22} \frac{2}{\pi^2 R} \left(\frac{p_i}{a}\right)$$

$$R_{31} = -R_{13}$$

$$R_{32} = R_{23} \qquad \text{(B.6)}$$

$$R_{33} = D_{11} \left(\frac{m}{a}\right)^4 - (2D_{12}+4D_{66}) \left(\frac{m}{a}\right)^2 \left(\frac{p_i}{a}\right)^2 + D_{22} \left(\frac{p_i}{a}\right)^4 - \frac{2B_{12}}{\pi^2 R} \left(\frac{m}{a}\right)^2$$

$$+ \frac{2B_{22}}{\pi^2 R} \left(\frac{p_i}{a}\right)^2 + \frac{A_{22}}{\pi^4 R^2} - \bar{N}_{11} \left(\frac{m}{a}\right)^2 \frac{1}{\pi^2} + \bar{N}_{22} \left\{ \frac{1}{\pi^2} \left(\frac{p_i}{a}\right)^2 - \frac{1}{\pi^4 R^2} \right\}$$

On expanding the determinant of the matrix [R] in equation (B.5), a characteristic polynomial is obtained as:

$$\bar{K}_8 p_i^8 + \bar{K}_6 p_i^6 + \bar{K}_4 p_i^4 + \bar{K}_2 p_i^2 + \bar{K}_0 = 0 \qquad \text{(B.7)}$$

The above equation thus yields eight values of p_i, which are real or complex conjugates. Four of these roots are the negatives of the other four.

Also, from equation (B.5):

$$U_i = \pi L_{2i} W_i$$

$$V_i = \pi L_{1i} W_i \qquad \text{(B.8)}$$

where

$$L_{1i} = \frac{R_{23} R_{11} - R_{13} R_{21}}{R_{21} R_{12} - R_{22} R_{11}} \qquad \text{(B.9)}$$

$$L_{2i} = \frac{R_{13} R_{22} - R_{23} R_{12}}{R_{21} R_{12} - R_{22} R_{11}} \qquad (B.9)$$

$$(i = 1, 2, \ldots 8)$$

After substituting equation (B.8) and the p_i values from equation (B.7) in equation (B.3), the displacements given by equation (B.1) are:

$$w = \sum_{i=1}^{8} e^{\beta_i} W_i \sin \alpha \qquad (B.10)$$

$$\theta = \sum_{i=1}^{8} \left\{ \frac{\pi p_i}{a} + \frac{1}{R} \pi L_{1i} \right\} e^{\beta_i} W_i \sin \alpha \qquad (B.11)$$

$$v = \sum_{i=1}^{8} \pi L_{1i} e^{\beta_i} W_i \sin \alpha \qquad (B.12)$$

$$u = \sum_{i=1}^{8} \pi L_{2i} e^{\beta_i} W_i \cos \alpha \qquad (B.13)$$

Similarly, substituting equation (A.1) in equations (A.5) and (A.6), the forces defined by equation (B.2) corresponding to the above displacements are:

$$\begin{aligned} \hat{Q} = \sum_{i=1}^{8} \Bigg[& - B_{12} \left(\frac{m}{a}\right)\left(\frac{p_i}{a}\right) \cdot \pi^3 L_{2i} + B_{22} \left\{ \left(\frac{p_i}{a}\right)^2 \pi^3 L_{1i} - \left(\frac{p_i}{a}\right) \frac{\pi}{R} \cdot \right\} \\ & + D_{12} \left(\frac{m}{a}\right)^2 \left(\frac{p_i}{a}\right) \cdot \pi^3 - D_{22} \left\{ \left(\frac{p_i}{a}\right)^3 \pi^3 + \left(\frac{p_i}{a}\right)^2 L_{1i} \frac{\pi^3}{R} \right\} \\ & - 2B_{66} \left\{ \left(\frac{m}{a}\right) \left(\frac{p_i}{a}\right) \pi^3 L_{2i} + \left(\frac{m}{a}\right)^2 \pi^3 L_{1i} \right\} \\ & + 4D_{66} \left\{ \left(\frac{m}{a}\right)^2 \left(\frac{p_i}{a}\right) \pi^3 + L_{1i} \frac{\pi^3}{R} \left(\frac{m}{a}\right)^2 \right\} \\ & - \bar{N}_{22} \left\{ \left(\frac{p_i}{a}\right) \cdot \pi + L_{1i} \frac{\pi}{R} \right\} \Bigg] e^{\beta_i} W_i \sin \alpha \end{aligned} \qquad (B.14)$$

$$\hat{M} = \sum_{i=1}^{8} \left[- B_{12} \left(\frac{m}{a}\right) L_{2i} \pi^2 + B_{22} \left\{ \left(\frac{p_i}{a}\right) \pi^2 L_{1i} - \frac{1}{R} \right\} \right.$$

$$\left. + D_{12} \left(\frac{m}{a}\right)^2 \pi^2 - D_{22} \left\{ \left(\frac{p_i}{a}\right)^2 \pi^2 + \left(\frac{p_i}{a}\right) L_{1i} \frac{\pi^2}{R} \right\} \right]. \qquad \text{(B.15)}$$

$$e^{\beta_i} W_i \sin \alpha$$

$$\hat{N} = \sum_{i=1}^{8} \left[-A_{12} \left(\frac{m}{a}\right) L_{2i} \pi^2 + A_{22} \left\{ \left(\frac{p_i}{a}\right) \pi^2 L_{1i} - \frac{1}{R} \right\} \right.$$

$$+ B_{12} \left(\frac{m}{a}\right)^2 \pi^2 - B_{22} \left\{ \left(\frac{p_i}{a}\right)^2 \pi^2 + \left(\frac{p_i}{a}\right) L_{1i} \frac{\pi^2}{R} \right\} \qquad \text{(B.16)}$$

$$\left. - \bar{N}_{22} \left\{ \left(\frac{p_i}{a}\right) \pi^2 L_{1i} - \frac{1}{R} \right\} \right] e^{\beta_i} W_i \sin \alpha$$

$$\hat{T} = \sum_{i=1}^{8} \left[A_{66} \left\{ \left(\frac{p_i}{a}\right) L_{2i} \pi^2 + \left(\frac{m}{a}\right) L_{1i} \pi^2 \right\} \right.$$

$$-2B_{66} \left\{ \left(\frac{p_i}{a}\right) \left(\frac{m}{a}\right) \cdot \pi^2 + \left(\frac{m}{a}\right) L_{1i} \frac{\pi^2}{R} \right\} \qquad \text{(B.17)}$$

$$\left. -\bar{N}_{22} \left(\frac{p_i}{a}\right) L_{2i} \pi^2 \right] e^{\beta_i} W_i \cos \alpha$$

Putting $y = \pm \frac{b}{2}$ in β_i of equation (B.3), equations (B.10) to (B.17) yield the displacements due to buckling and the corresponding forces along the two sides of the laminated curved plate-strip element. Figure 18 shows their positive directions. It is pointed out that all quantities are mid plane values, chosen here as the reference plane, and are with respect to the local axes system. The above displacements and forces are functions of the axial half-wave length of buckling $(\frac{a}{m})$ and the biaxial loading, $\bar{N}_{11}$ and $\bar{N}_{22}$.

In idealizing a structure of uniform cross section as an assembly of element types discussed in Appendix A, offsets between elements necessitates an appropriate offset transformation. Also, the intersecting angle between elements being arbitrary, it is convenient to transform all

displacements and forces to common global axes. These two transformations are now considered.

Figure 19 shows the offsets to S of the side B of the plate-strip element AB. Axes system x_s, y_s and z_s at S are chosen parallel to the local axes at B. Offsets at the side A are considered in a similar manner. The offsets are defined by the distances y_0 and z_0 measured along the local y and z axes, respectively, from the side of the plate-strip element in the reference plane. The offsets are positive when they are in the positive directions of the local axes. The displacements of equations (B.10) to (B.13) on transformation to the axes through S, become:

$$w_s = w + y_0 \theta \tag{B.18}$$

$$\theta_s = \theta \tag{B.19}$$

$$v_s = v - z_0 \theta \tag{B.20}$$

$$u_s = u - \underline{z_0 \; w_{,x}} - \underline{y_0 \; v_{,x}} \tag{B.21}$$

The above equations represent a rigid body transfer when the underlined terms in equation (B.21) are dropped. Physically, these underlined terms signify that there is no relative slippage between B and S along the x-axis. Substituting for w, θ, v and u from equations (B.10) to (B.13), the equations (B.18) to (B.21) are written in matrix form as:

$$d_s = C_1 X_1 W_i \tag{B.22}$$

where

$$d_s = \begin{Bmatrix} w_s \\ \theta_s \\ v_s \\ u_s \end{Bmatrix} ; \quad W_i = \begin{Bmatrix} W_1 \\ . \\ . \\ W_8 \end{Bmatrix} \tag{B.23}$$

$$C_1 = \lceil \sin\alpha, \; \sin\alpha, \; \sin\alpha, \; \cos\alpha \rfloor \tag{B.24}$$

X_1 is a 4 x 8 matrix whose elements are functions of geometric and material properties of the curved plate-strip element, the p_i values and the axial half-wave length of buckling ($\frac{a}{m}$).

The forces in equations (B.14) to (B.17) when transferred to the axes system through S, become:

$$\hat{Q}_s = Q - \underline{z_0 T_{,x}} \tag{B.25}$$

$$\hat{M}_s = M + y_0 Q - z_0 N \tag{B.26}$$

$$\hat{N}_s = N - \underline{y_0 T_{,x}} \tag{B.27}$$

$$\hat{T}_s = T \tag{B.28}$$

The underlined terms in the above equations are similar to those in equation (B.21). Substituting for Q, M, N and T from equations (B.14) to (B.17), the above equations are written as:

$$f_s = C_1 X_2 W_i \tag{B.29}$$

where $$f_s = \begin{Bmatrix} \hat{Q}_s \\ -\hat{M}_s \\ \hat{N}_s \\ \hat{T}_s \end{Bmatrix} \tag{B.30}$$

In the force vector f_s above, a negative sign is used with M_s in order to reverse the direction of the moment as given by equation (B.26). As will be apparent later, this facilitates the use of a common coordinate transformation matrix for all the element types included in the present analysis. The vector W_i and the diagonal matric C_1 are defined in equations (B.23) and (B.24). X_2 is a 4 x 8 matrix similar to the X_1 matrix discussed previously..

Figure 19 shows arbitrarily chosen global axes x_G, y_G and z_G. Also shown are positive directions of the global displacements and forces, subscripted G. Since the axes system x_s, y_s and z_s at any offset point is parallel to the local axes system along the corresponding side, (A or B), the transformation angle to the global axes at A is:

$$\phi_A = \psi - \frac{\zeta}{2} \tag{B.31}$$

and at B,

$$\phi_B = \psi + \frac{\zeta}{2} \tag{B.32}$$

The angle is measured positive in the clockwise direction, from the global axes. For a flat plate-trip element $\phi_A = \phi_B = \psi$.

A matrix $\tilde{T}_0$ for coordinate transformation through angle ϕ, is defined as:

$$\tilde{T}_0 = \begin{bmatrix} \cos\phi & 0 & \sin\phi & 0 \\ 0 & 1 & 0 & 0 \\ -\sin\phi & 0 & \cos\phi & 0 \\ 0 & 0 & 0 & 1 \end{bmatrix} \tag{B.33}$$

Superscripts - and + are used hereafter to denote the two sides of the curved plate-strip element identified by the values of $y = -\frac{b}{2}$ and $y = +\frac{b}{2}$, respectively, in β_i of equations (B.3). The displacements and forces along these two sides, on using equations (B.22) and (B.29) and on transformation to the global axes, become:

$$\begin{Bmatrix} d_G^- \\ \hline d_G^+ \end{Bmatrix} = \left[\begin{array}{c|c} \tilde{T}_A & 0 \\ \hline 0 & \tilde{T}_B \end{array}\right] \left[\begin{array}{c|c} C_1 & X_1^- \\ \hline C_1 & X_1^+ \end{array}\right] \begin{Bmatrix} W_i \end{Bmatrix} = C_2 X_3 W_i \tag{B.34}$$

$$\begin{Bmatrix} f_G^- \\ \hline f_G^+ \end{Bmatrix} = \left[\begin{array}{c|c} -\tilde{T}_A & 0 \\ \hline 0 & \tilde{T}_B \end{array}\right] \left[\begin{array}{c|c} C_1 & X_2^- \\ \hline C_1 & X_2^+ \end{array}\right] \begin{Bmatrix} W_i \end{Bmatrix} = C_2 X_4 W_i \tag{B.35}$$

where $C_2 = \begin{bmatrix} C_1 & 0 \\ 0 & C_1 \end{bmatrix}$

$\tilde{T}_A$ and $\tilde{T}_B$ are the coordinate transformation matrices obtained from equation (B.33) for angles ϕ_A of equation (B.31) and ϕ_B of equation (B.32), respectively. The negative sign associated with $\tilde{T}_A$ in equation (B.35) is a consequence of the sign convention for forces in the local axes system. The 8 x 8 matrices X_3 and X_4 are self-explanatory.

The axial (x) distributions of the above buckling displacements and the corresponding forces are trigonometric functions (sin or cos) of α $(= \frac{m\pi x}{a})$ as seen from the C_2 matrix. The beam elements also have identical distributions, as will be seen in sub-section B.2. This is due to the need for the number of axial (x) half-waves of buckling, m, to be identical in all elements making up the structure. Hence the C_2 matrix can be separated out and readily dropped from further consideration.

Substituting for W_i from equation (B.34) into equation (B.35), the stiffness matrix [s] of the laminated curved plate-strip element is obtained from:

$$\begin{Bmatrix} f_G^- \\ f_G^+ \end{Bmatrix} = \begin{bmatrix} & s & \end{bmatrix} \begin{Bmatrix} d_G^- \\ d_G^+ \end{Bmatrix} \qquad \text{(B.36)}$$

$$\text{where } [s] = \begin{bmatrix} s_{11} & s_{12} \\ s_{21} & s_{22} \end{bmatrix} = X_4 (X_3)^{-1} \qquad \text{(B.37)}$$

$$\text{and } s_{21} = s_{12}^T \qquad \text{(B.38)}$$

[s] is symmetric and defines the global relationship between the buckling displacements and the corresponding forces along the sides $y = -\frac{b}{2}$ and $y = +\frac{b}{2}$ of the curved plate-strip element, taking into account any offsets.

The elements of this matrix are transcendental functions of the half-wave length of buckling $(\frac{a}{m})$ and the applied loads $\bar{N}_{11}$ and $\bar{N}_{22}$.

In the structures for which the present buckling analysis is applicable, some of the individual plate-strip elements have specified boundary conditions (e.g., simply supported, clamped, free, etc.) along an external longitudinal (x) side, not connected to other elements. Such conditions are treated here in a general manner as elastic restraints (specified as spring constants) to freedoms corresponding to displacements w, θ, v and u. A diagonal matrix k_o is defined as

$$k_o = \lceil k_w, k_\theta, k_v, k_u \rfloor \tag{B.39}$$

where k_w, k_θ, k_v and k_u are the spring constants in the directions of the subscripted displacements, with reference to the local axes system x, y and z. If there is complete freedom in one direction, the corresponding spring stiffness is zero. Similarly, if there is complete restraint in one direction the corresponding spring stiffness is theoretically infinite. In numerical computations, a sufficiently large number is used for infinite spring stiffness to avoid numerical problems.

Consider the side of the curved plate-strip element along B ($y = + \frac{b}{2}$) in figure 19 being elastically restrained by the specified spring stiffness of equation (B.39). These are transformed to the global axes system as:

$$k_G^+ = \tilde{T}_B \, k_o \, (\tilde{T}_B)^{-1} \tag{B.40}$$

Then, $$f_G^+ = - k_G^+ \, d_G^+ \tag{B.41}$$

Also, from equations (B.36) and (B.37)

$$f_G^+ = s_{21} \, d_G^- + s_{22} \, d_G^+ \tag{B.42}$$

Combining the above two equations

$$d_G^+ = - (s_{22} + k_G^+)^{-1} \, s_{21} \, d_G^- \tag{B.43}$$

Equations (B.36) and (B.37) also yield:

$$f_G^- = s_{11} \, d_G^- + s_{12} \, d_G^+ \tag{B.44}$$

Substituting equation (B.43), in the above:

$$f_G^- = s_A \, d_G^- \tag{B.45}$$

where the 4x4 reduced stiffness matrix s_A for the curved plate-strip element, relating the forces and displacements along the side A ($y = -\frac{b}{2}$), with the side B ($y = +\frac{b}{2}$) elastically restrained, is given by:

$$s_A = s_{11} - s_{12} \, (s_{22} + k_G^+)^{-1} \cdot s_{21} \tag{B.46}$$

When the side A is elastically restrained instead of the side B, the equations derived in an analogous manner are:

$$k_G^- = \tilde{T}_A \, k_o \, (\tilde{T}_A)^{-1} \tag{B.47}$$

$$f_G^+ = s_B \, d_G^+ \tag{B.48}$$

$$s_B = s_{22} - s_{21} \, (s_{11} + k_G^-)^{-1} \, s_{12} \tag{B.49}$$

In equations (B.45) and (B.48) the axial (x) distributions of the displacments and forces are separated out, for reasons discussed earlier.

In the limit as the radius $R \to \infty$, the above equations for the curved plate-strip element degenerate to those of a flat plate-strip element. In the latter case, some further simplifications aiding in numerical solution are possible, when the elements of the coupling matrix [B] in equations (A.5) and (A.6) are identically zero.

Laminated flat plates with mid-plane symmetry and isotropic flat plates are typical examples of such cases. The simplifications are outlined in Appendix D.

B.2 Stiffness of Beam Elements

The assumed buckling displacement functions for the beam element are:

$$w = W_b \sin \alpha$$

$$\theta = \Theta_b \sin \alpha \tag{B.50}$$

$$v = V_b \sin \alpha$$
$$u = U_b \cos \alpha \qquad \text{(B.50)}$$

where $\alpha = \frac{m\pi x}{a}$ as in equation (B.3). The above functions are chosen to satisfy the simply supported boundary conditions at the ends $x = 0$ and $x = a$.

On substituting the above displacement functions in equations (A.29) to (A.32), the corresponding forces in the beam element under axial compression $\bar{P}_b$, are:

$$f_b = X_5 \, d_b \qquad \text{(B.51)}$$

where

$$f_b = \begin{Bmatrix} q_z \\ \frac{dM_x}{dx} \\ q_y \\ \frac{dP}{dx} \end{Bmatrix} \quad ; \quad d_b = \begin{Bmatrix} w \\ \theta \\ v \\ u \end{Bmatrix} \qquad \text{(B.52)}$$

$$X_5 = \begin{bmatrix} a_{11} & a_{12} & 0 & 0 \\ & a_{22} & a_{23} & 0 \\ & & a_{33} & 0 \\ & \text{SYM} & & a_{44} \end{bmatrix} \qquad \text{(B.53)}$$

$$a_{11} = E_{11}\, I_{yy}\, (\frac{m\pi}{a})^4 - \overline{P}_b\, (\frac{m\pi}{a})^2$$

$$a_{12} = -\overline{P}_b\, y_m\, (\frac{m\pi}{a})^2$$

$$a_{22} = E_{11}\, \Gamma\, (\frac{m\pi}{a})^4 - (\bar{\sigma}\, I_p - G_{23}\, J)\, (\frac{m\pi}{a})^2 \qquad \text{(B.54)}$$

$$a_{23} = + \overline{P}_b\, z_m\, (\frac{m\pi}{a})^2$$

$$a_{33} = E_{11}\, I_{zz}\, (\frac{m\pi}{a})^4 - \overline{P}_b\, (\frac{m\pi}{a})^2$$

$$a_{44} = E_{11}\, A_b\, (\frac{m\pi}{a})^2$$

The above displacements and forces are defined with respect to the local axes x, y and z through the shear center 0. Their positive directions are shown in Figure 17.c. For reasons discussed in subsection B.1 for the plate-strip elements, it is possible to separate out the axial distribution of these displacements and forces and eliminate it from further consideration.

An offset tranformation identical to that for the plate-strip element, equations (B.18) to (B.21) and (B.25) to (B.28), can be readily done. However, it is not pursued here as the offsets in plate-strip elements would suffice for the idealization of the types of structures considered.

Let the angle, measured positive in the clockwise direction, from the global axes to the local beam element axes be ϕ_b. Then using the coordinate transformation matrix $\tilde{T}_b$ from equation (B.33), for the angle ϕ_b, the beam element forces are tranformed to the global axes as:

$$f_{bG} = \tilde{T}_b\, X_5\, \tilde{T}_b^{-1}\, d_{bG} \qquad \text{(B.55)}$$

or $\quad f_{bG} = s_b\, d_{bG}$

where s_b is the beam element stiffness matrix (4x4). The elements of this matrix are functions of $\overline{P}_b$, the axial compressive load in the beam element, and the axial half-wavelength of buckling $(\frac{a}{m})$.

B.3 Buckling Formulation

The equations developed thus far are now applied in formulating the buckling criterion for an arbitrary structure of uniform cross-section. The structure shown in Figure 20 is chosen as the example. The longitudinal (x) sides along G and H are arbitrarily restrained. This structure is readily idealized as an assemblage of:

(a) curved plate-strip elements - 2, 3 and 9

(b) flat plate-strip elements - 1, 4, 5, 7, 8 and 11

(c) beam elements - 6 and 10

In the figure, the element numbers are shown circled. The broken line is drawn through the mid-plane of the plate-strip elements. The extremities of each plate-strip element and the shear center of each beam type element are marked with "dots." x_G, y_G and z_G are the chosen global axes; x_G coinciding with the axis of the structure. y and z are the local axes in each element. The local x axis, (not shown in the figure) is parallel to x_G. The idealization of the structure, as indicated above, also defines any offsets between elements. It is possible to differentiate between bonded and riveted connections. Ref. 9 gives details of the idealization procedure for any structure.

Subsections B.1 and B.2 give the equations for the stiffness matrices of individual elements, with respect to the global axes system. These are:

(i) equations (B.45) and B.48) for the reduced stiffness matrix of plate-strip elements with specified boundary conditions along one external longitudinal (x) side

(ii) equation (B.36) for the stiffness matrix of any other plate-strip element

(iii) equation (B.55) for the stiffness matrix of beam elements.

It is obvious that to evaluate the above stiffnesses, it is necessary to know the loadings on each element corresponding to any chosen level of total external load on the structure. These element loadings are dictated by considerations of strain compatibility between elements and as shown in subsection B.4, in general, vary from element to element.

The above element matrices are merged appropriately to form the stiffness matrix of the total structure. The merging process is identical to that in the direct stiffness method of finite element analysis,

where the buckling formulation is

$$K \cdot D = 0 \tag{B.56}$$

or

$$(K_o + \lambda K_g) \cdot D = 0 \tag{B.57}$$

K_o is the usual elastic stiffness matrix, K_g is the geometric stiffness matrix and D is the buckling displacement vector.

The corresponding equation for the analysis presented here is:

$$S \cdot D = 0 \tag{B.58}$$

where the merged symmetric matrix S is similar to K in equation (B.56). However, S is not separable in the form of equation (B.57) because of the manner in which the stiffness matrix of each element is derived from the exact analytical displacement solutions. D is now the vector representing the global buckling displacements of inter-element junction lines. As already indicated in subsections B.1 and B.2, the axial (x) distribution of the displacements and forces has been separated out. Hence, the vector D has implied values of sin α and cos $\alpha = 1$. It is obvious that equation (B.58) signifies the equilibrium of the structure in an adjacent deflected (buckled) position, while satisfying all the boundary conditons and inter-element conditions. A non-trivial solution to this equation is obtained when the matrix S has a zero determinant, i.e.,

$$| S | = 0 \tag{B.59}$$

The elements of S are transcendental functions of the external loadings and the axial (x) half-wavelength of buckling $(\underline{a})$. Thus the above equation does not correspond to the standard algebraic eigenvalue problem.

For any chosen number of axial half-waves m, the lowest level of external loading at which equation (B.59) is satisfied, is the buckling load of the structure. This load is determined by the iteration procedure discussed in Appendix C. A series of m values are investigated and the the lowest of all buckling loads then gives the critical load of the structure. The corresponding vector D in equation (B.58), giving the inter-element junction line displacements, is then obtained by Wielandt's method of inverse iteration, Ref. 17. The convergence of this method is good but is dependent on the accuracy of the solution to equation (B.59).

The distribution of the buckling displacements across the width of each plate-strip element is calculated from equation (B.3). The necessary W_i values for each element are obtained by back-substituting into equation

(B.34) the corresponding d_G^- and d_G^+ values from the eigenvector D. The U_i and V_i values follow from equation (B.8). For the beam elements, the eivenvector D directly gives the global buckling displacements at the shear center. These can be readily transformed back to the local axes system.

The w and v buckling displacements of each element are of prime interest. A plot showing these displacements across the cross section of the structure identifies the weak (buckled) elements and thereby indicates whether the buckling is local or general. Such plots give a valuable insight into the buckling mechanism and may be used in achieving efficient design of structures as illustrated in Refs. 1 and 2 for stiffened panels.

The classical buckling analysis usually makes assumptions regarding individual buckling modes, like Euler mode, torsional mode, local mode, etc. As shown in Ref. 2 such simplifying assumptions could sometimes lead to the possibility of missing the lowest buckling load. Apart from the need for the number of buckling half-waves, m, in the longitudinal (x) direction, to be the same in all elements of the structure, the present analysis makes no other assumptions regarding the buckle mode.

B.4 Element Loadings for a Specified Load in the Structure

The buckling analysis requires the knowledge of the distribution of the total load on the structure between the various elements. This is determined from considerations of strain compatibility between elements. As a consequence of ignoring the pre-buckling deformations, at buckling each element in the structure is under uniform load conditions. Thus, each plate-strip element is, in general, under uniform biaxial loading $\bar{N}_{11(j)}$ and $\bar{N}_{22(j)}$ and the beam element under uniform axial load $\bar{P}_{b(k)}$, (j) and (k) referring to the element numbers.

For plate-strip elements, noting that there are no applied moments, equations (A.5) and (A.6) are combined to give:

$$\bar{N} = [\bar{A} - \bar{B}\,(\bar{D})^{-1}\,\bar{B}]\,\bar{\epsilon}^{\circ} \tag{B.60}$$

or in the expanded form

$$\bar{N}_{11} = \bar{C}_{11}\,\bar{\epsilon}_x^{\circ} + \bar{C}_{12}\,\bar{\epsilon}_y^{\circ} \tag{B.61}$$

$$\bar{N}_{22} = \bar{C}_{12}\,\bar{\epsilon}_x^{\circ} + \bar{C}_{22}\,\bar{\epsilon}_y^{\circ} \tag{B.62}$$

where

$$\bar{A} = \begin{bmatrix} A_{11} & A_{12} \\ A_{12} & A_{22} \end{bmatrix} \quad ; \quad \bar{B} = \begin{bmatrix} B_{11} & B_{12} \\ B_{12} & B_{22} \end{bmatrix} \quad ; \quad \bar{D} = \begin{bmatrix} D_{11} & D_{12} \\ D_{12} & D_{22} \end{bmatrix}$$

The coefficients $\bar{C}_{11}$, $\bar{C}_{12}$ and $\bar{C}_{22}$ are self-evident. On inverting, the above equations yield:

$$\bar{\varepsilon}_x^\circ = \bar{F}_{11}\,\bar{N}_{11} + \bar{F}_{12}\,\bar{N}_{22} \tag{B.63}$$

$$\bar{\varepsilon}_y^\circ = \bar{F}_{12}\,\bar{N}_{11} + \bar{F}_{22}\,\bar{N}_{22} \tag{B.64}$$

The coefficients $\bar{F}_{11}$, $\bar{F}_{12}$ and $\bar{F}_{22}$ are readily derived.

For a laminated beam element with k layers, the axial load corresponding to an axial strain $\bar{\varepsilon}_x^\circ$ is given by

$$\bar{P}_b = \bar{\varepsilon}_x^\circ \sum_{k=1}^{\ell} E_{11}^{\,k} A_b^{\,k} \tag{B.65}$$

The above equations are used in the strain compatibility considerations. The method is discussed below with reference to the stiffened panel in Figure 21. The numbers in parenthesis are the element numbers.

(i) Biaxial loading with constant inplane transverse load along the panel sides.-The panel has a specified transverse loading of $\bar{N}_{22(1)}$ along the external side of element (1). This remains constant as the axial load on the panel is increased. From statics it is evident that $\bar{N}_{22(j)}$ for any plate-strip element (j) on the skin is identical to $\bar{N}_{22(1)}$. For element (1), at a chosen value of $\bar{N}_{11(1)}$ and the specified $\bar{N}_{22(1)}$, the corresponding strain $\bar{\varepsilon}_{x\,(1)}^\circ$ follows from equation (B.63). At any level of axial load in the panel the axial strain $\bar{\varepsilon}_{x\,(1)}^\circ$ in any element is made identical to $\bar{\varepsilon}_{x(1)}^\circ$. Thus, applying equation (B.63) to any plate-strip element (j),

$$\bar{N}_{11(j)} = \frac{1}{\bar{F}_{11(j)}}\,\bar{\varepsilon}_{x(1)}^\circ - \bar{F}_{12(j)}\,\bar{N}_{22(j)} \tag{B.66}$$

In the above equation $\bar{N}_{22(j)}$ is obviously zero for those plate-strip elements in the panel not carrying any side load. Equation (B.65) gives the axial load in the beam elements corresponding to the strain $\bar{\varepsilon}^{\circ}_{x(1)}$. Thus, for any chosen $\bar{N}_{11(1)}$ and a specified constant value of $\bar{N}_{22(1)}$, the corresponding loadings in all elements are known. The total load in the structure in either direction can be easily calculated.

(ii) Biaxial loading with constant axial strain.--The specified axial strain $\bar{\varepsilon}^{\circ}_{x(1)}$ is the same for all elements in the panel ($\bar{\varepsilon}^{\circ}_{x(j)} = \bar{\varepsilon}^{\circ}_{x(1)}$) and remains constant. For a chosen value of $\bar{N}_{22(1)}$ (by statics $\bar{N}_{22(j)} = \bar{N}_{22(1)}$ for all plate-strip elements on the skin) Equation (B.62) gives

$$\bar{\varepsilon}^{\circ}_{y(j)} = \frac{1}{\bar{C}_{22(j)}} \left[\bar{N}_{22(j)} - \bar{C}_{12(j)} \; \bar{\varepsilon}^{\circ}_{x(j)} \right] \tag{B.67}$$

The axial loading $\bar{N}_{11(j)}$ in all plate-strip elements follows from equation (B.61) and the loads in the beam elements from equation (B.65).

(iii) Biaxial loading with constant total axial load.--Initially, $\bar{N}_{22(j)}$ is zero and for a specified value of $\bar{N}_{11(1)}$ equation (B.63) gives

$$\bar{\varepsilon}^{\circ}_{x(1)} = \bar{F}_{11(1)} \, \bar{N}_{11(1)} \tag{B.68}$$

The axial loading $\bar{N}_{11(j)}$ in all other plate-strip elements at this strain value is:

$$\bar{N}_{11(j)} = \frac{\bar{F}_{11(1)} \, \bar{N}_{11(1)}}{\bar{F}_{11(j)}} \tag{B.69}$$

The axial load in beam elements follows from equation (B.65). The total axial load defined by the axial loads in all elements determined as above is kept constant at all levels of inplane transverse loading.

(iv) Biaxial loading at constant biaxial load ratio.--A biaxial load ratio defined by $\bar{N}_{11(1)}/\bar{N}_{22(j)}$ is specified and remains constant. Thus, at a chosen value of $\bar{N}_{11(1)}$ the corresponding value of $\bar{N}_{22(1)}$ is known. Equation (B.63) gives the corresponding axial strain $\bar{\varepsilon}^{\circ}_{x(1)}$, which is the same in all elements ($\bar{\varepsilon}^{\circ}_{x(j)} = \bar{\varepsilon}^{\circ}_{x(1)}$). Also, the above calculated $\bar{N}_{22(1)}$ is the same in all plate-strip elements on the skin. Then from equation (B.63)

$$\bar{N}_{11(j)} = \frac{1}{\bar{F}_{11(j)}} \left[\bar{\varepsilon}^{\circ}_{x(1)} - \bar{F}_{12(j)} \bar{N}_{22(j)} \right] \qquad (B.70)$$

As before the corresponding axial load in each beam element is calculated from equation (B.65)

APPENDIX C

SOME SOLUTION METHODS AND NUMERICAL PHENOMENA OF PARTICULAR INTEREST

This appendix summarizes some of the numerical solution methods used in the buckling analysis presented in Section 5 as well as interesting numberical phenomena observed.

C.1 Buckling Load Evaluation

Equation (B.57), for the buckling load evaluation, represents a general non-linear eigenvalue problem, for the reasons mentioned in sub-section B.3. Recourse to an iterative procedure is necessary to determine the lowest buckling load for a particular number m of axial (x) half-wave lengths. The often-used method of determinant plotting risks missing the lowest root and may also be time-consuming. Because of the symmetry of the matrix S, the algorithm outlined below enables the lowest root (buckling load) to be determined with certainty in fewer iterations. The principle of the algorithm is analogous to methods based on the Sturm sequence property, Ref. 17, for standard algebraic eigenvalue problems.

Assume that all inter-element junction lines are completely restrained against the degrees of freedom represented by the vector D in equation (B.58). Each element making up the structure can thus be considered as isolated with clamped boundary conditions along these restrained lines. Specified boundary conditions along any external longitudinal (x) side of plate-strip elements are kept unchanged. For the chosen value of m, it is possible to determine a buckling load P_r for each element isolated as above.

Let P_{trial} be the current, trial value of the external load in the iteration process and let η_o be the total number of P_r values lower than P_{trial}. The imposed restraints along the inter-element junction lines are now released, one by one. Using the principles stated in Ref. 26 for the vibration frequencies of linearly elastic structures, it can be shown that the removal of each restraint either increases η_o by one or leaves it unchanged. The alternatives are decided from the decomposition of the symmetric matrix S, (using a modified Gaussian elimination method without row interchanges) into

$$S = L\, D_o\, L^T \qquad (C.1)$$

where D_o is a diagonal matrix, L is a unit lower triangular matrix and L^T is the transpose of L. A negative element in D_o signifies that the release of restraint to the freedom represented by the corresponding element in the vector D of equation (B.58) increases η_o by one. If it is positive, η_o remains unchanged.

Let η_s be the number of negative elements (also called sign count) in D_o and η be the number of roots of equation (B.57) below the value P_{trial}. Then, the principle of the algorithm used for buckling load evaluation is basically:

$$\eta = \eta_o + \eta_s \tag{C.2}$$

The lowest buckling load P_m for the chosen m corresponds to the value of P_{trial} (determined to the desired accuracy), at which η changes from zero to one. The algorithm is described in detail in Ref. 7. In the presence of coincident roots, it is obviously not possible to isolate a load at which η changes from zero to one. This is further discussed in sub-section C.3. From the above discussion it is seen that a reliable method of calculating P_r is crucial to the success of the algorithm. Also, P_m cannot exceed P_u, the smallest of the P_r values. P_u is thus an upper bound to P_m. For any chosen m value there is a corresponding upper bound load P_u. The method used to calculate the P_r values and hence P_u, is discussed in Appendix E. Ensuring P_{trial} to be always less than P_u results in η_o being zero. The smallest root (buckling load P_m) of equation (B.59) is then the lowest value of P_{trial} (determined to the desired accuracy), at which η_s changes from zero to one. If for some particular reason one is interested in a specific higher root, it is obvious that it is readily determined by finding the value of P_{trial} at which the corresponding change occurs in η_o. It is seen from equation (C.1) that

$$|S| = |D_o| = \prod_i d_{ii} \tag{C.3}$$

since

$$|L| = |L^T| = 1.$$

C.2 Open Structures With Repeated Substructures

Open structures with repeated substructures are exemplified by stiffened panels, with repetition in regard to the stiffeners (substructure) and their spacing, as shown in Figure 22. All repeated substructures are identical. The boundary conditions along the two sides of the panel are arbitrary. There is no restriction on the type of substructures and they may be multiply connected. The symmetric matrix S in equation (B.58) for such "open structures" is banded and has a typical block structure as shown in Figure 23. Each block marked CR represents one repeated substructure. In flat stiffened panels every repeated substructure is identically oriented with respect to the global axes. All repeat blocks CR are, thus identical in every respect. However, in curved stiffened panels with constant curvature, (of the type shown in Figure 1.f), the orientation of each substructure with respect to the global axes increments by a constant angle from substructure to substructure. In such cases the repeat blocks have identical dimensions only, while the elements of one are readily obtained from the elements of the other using a transformation matrix.

Stiffened cylinders, even though they have repeated substructures (stiffeners), do not come under the purview of "open structures." The matrix S for these "closed structures" is no longer banded, as the first and the last elements making up the structure are inter-connected.

The above discussed characteristics of open structures (with repeated sub-structures) is made use of in the method, Refs. 27 and 28, for calculating η_o, the number of negative elements in the diagonal matrix D_o of equation (C.1). With reference to Figure 23, physical considerations dictate that (M-N) columns of the CR matrices overlap. The elimination procedure used is illustrated in Figure 24. Starting with block CS, the elements below the first IR diagonal elements are eliminated (step 1 of Figure 24). The product of the first IR diagonal elements comprises the first IR terms in equation (C.3). The first IR rows and columns are discarded after this product is computed. The remaining rectangular block CS_2 is moved into the upper left-hand corner, and the first CR block is brought into position as shown in step 2 of Figure 24. This step is completed after the elements below the first N diagonal elements of the composite matrix are annihilated and the product of these diagonal terms included in the running product of equation (C.3). The procedure continues in the manner shown in Figure 24. It differs from the usual elimination procedure only in that information is discarded from the working array when it is no longer needed, and new information is brought into this array only when needed to continue the process. This scheme minimizes the computer core storage requirements. The number of repeat blocks, while mathematically arbitrary, will be limited in practice by the accumulation of rounding errors.

C.3 Coincident Roots

In shell buckling problems the method of determinant plotting is often used. The buckling load is identified by the sign reversal in the determinant value. In certain cases the phenomenon of "kissing" determinant[1] has been observed. The determinant value decreases rapidly to a near zero value, within numerical limits, and then increases again without going through a sign reversal. This occurs in spite of using extremely small load intervals. This phenomenon is caused by coincident roots and can entail the possibility of missing the lowest buckling load, unless special precautions are taken. The significance of the coincident roots in regard to the buckling analysis presented in Appendix B, is discussed below. The algorithm based on equation (C.2) defines the buckling load as that value of P_{trial} (determined to the desired accuracy) at which η (or η_s when the upper bound load P_u is used) changes from zero to one. Whenever equation (B.57) has coincident roots it is not possible to isolate such a value of P_{trial}. This is brought out by the examples of the thin-walled cylinder and the long square tube discussed in sub-section 5.4. In spite of pursuing the load iteration to the single precision accuracy of the CDC 6600 computer, these cases did not reveal a zero to one, but only a zero to two change in η value. A closer look at the structures shows the possibility of buckling modes with coincident buckling loads, the corresponding eigenvectors D in equation (B.58) for these modes being mutually orthogonal. Thus, this change in the η value reflects the existence of the coincident roots. For such cases, the algorithm outlined in subsection C.1 still yields the smallest root of equation (B.59), with certainty. The eigenvector solution method used yields one of the modes. However, it is possible to evaluate the orthogonal vectors using special numerical techniques, Refs. 17 and 18. For the class of structures for which the present analysis is intended, such techniques are not warranted from an engineering point of view. The coincident roots can be separated into distinct ones by introducing a small "error" (change in the modelling of the structure), with insignificant effect on the basic structural characteristics or results. This is illustrated in subsection 5.4.

C.4 Complex Conjugate p_i Roots

It is seen from subsection B.1 that the complex roots p_i of the characteristic equation (B.7) appear in pairs which are complex conjugates. The use

---

[1] This was brought to the attention of the authors by Dr. M. F. Card, Structures Division, NASA, Langley Research Center, Hampton, Virginia 23365.

of such a pair of p_i values in equations (B.10) to (B.17) results in a complex conjugate pair of columns in the matrices X_1 and X_2 of equations (B.22) and (B.29).

For each p_i value there is obviously a corresponding element in the vector W_i of equations (B.22), (B.29), (B.34) and (B.35). Further, it can be shown that the elements of W_i corresponding to a complex conjugate pair of p_i, are themselves complex conjugates.

Thus, if a typical complex conjugate pair of elements in X_1 or X_2 are $(c + id)$ and $(c - id)$, with the corresponding elements in the vector W_i being $(r + is)$ and $(r - is)$, the result of multiplying them out is seen to be a real number. It follows that the matrices X_1 and X_2 can be manipulated to contain only real numbers, with a corresponding change in the elements of the vector W_i. This simplification is used in the numerical solution.

APPENDIX D

FLAT PLATE-STRIP ELEMENTS WITH ZERO BENDING-STRETCHING COUPLING

For flat plate-strip elements, the simplifications given below aid the numerical solution when the elements of the coupling matrix [B] in equations (A.5) and (A.6) are identically zero.

The buckling displacements are assumed as (cf. equation (B.3))

$$w = \sum_{i=1}^{4} W_i e^{\beta_{1i}} \sin\alpha \tag{D.1}$$

$$v = \sum_{i=1}^{4} V_i e^{\beta_{2i}} \sin\alpha \tag{D.2}$$

$$u = \sum_{i=1}^{4} U_i e^{\beta_{2i}} \cos\alpha \tag{D.3}$$

where $\beta_{1i} = \frac{p_{wi}\pi y}{a}$

$$\beta_{2i} = \frac{p_{ui}\pi y}{a}$$

$$\alpha = \frac{m\pi x}{a}$$

P_{wi} and P_{ui} are the roots of two separate characteristic equations, as shown below.

With $B_{11} = B_{22} = B_{12} = B_{66} = 0$, the equations (A.13) and (A.14) are uncoupled from equation (A.15). This is seen from equation (B.6) where substituting the above values and dropping the terms involving the radius R, results in $R_{13} = R_{23} = R_{31} = R_{32} = 0$. In R_{11}, R_{12}, R_{21}, and R_{22} of equation

(B.6), p_i is replaced with p_{ui} and in R_{33}, p_i is replaced with p_{wi}. Due to this uncoupling, equation (B.5) is written as:

$$\begin{bmatrix} R_{11} & R_{12} \\ R_{21} & R_{22} \end{bmatrix} \begin{Bmatrix} U_i \\ V_i \end{Bmatrix} = 0 \tag{D.4}$$

and

$$R_{33}\, W_i = 0 \tag{D.5}$$

The determinant of the coefficient matrix in equation (D.4) yields the characteristic polynominal:

$$\bar{K}_{u4} p_{ui}^{\,4} + \bar{K}_{u2} p_{ui}^{\,2} + \bar{K}_{u0} = 0 \tag{D.6}$$

The four p_{ui} roots from this equation are used in equations (D.2) and (D.3) for the inplane displacements v and u, respectively. Also, from equation (D.4),

$$V_i = L_{3i}\, U_i \tag{D.7}$$

where

$$L_{3i} = -\frac{R_{11}}{R_{12}} = -\frac{R_{21}}{R_{22}} \tag{D.8}$$

$(i = 1, 2, 3, 4)$

A second characteristic polynomial resulting from equation (D.5) is,

$$R_{33} = 0 \tag{D.9}$$

R_{33} is a fourth order polynomial in p_{wi}, containing even powers of p_{wi}. The four p_{wi} roots of equation (D.9) are used in equation (D.1) for the out-of-plane displacement w.

The roots p_{ui} and p_{wi} from equations (D.6) and (D.9), respectively, are always real or complex conjugates. Using these roots, equations corresponding to those of (B.10) to (B.17) are written as:

$$w = \sum_{i=1}^{4} e^{\beta_{1i}} W_i \sin \alpha \tag{D.10}$$

$$\theta = \sum_{i=1}^{4} \frac{\pi p_{wi}}{a} e^{\beta_{1i}} W_i \sin \alpha \tag{D.11}$$

$$v = \sum_{i=1}^{4} L_{3i} e^{\beta_{2i}} U_i \sin \alpha \tag{D.12}$$

$$u = \sum_{i=1}^{4} e^{\beta_{2i}} U_i \cos \alpha \tag{D.13}$$

$$\hat{Q} = \sum_{i=1}^{4} \left[D_{12}\left(\frac{m}{a}\right)^2 \left(\frac{p_{wi}}{a}\right)\pi^3 - D_{22}\left(\frac{p_{wi}}{a}\right)^3 \pi^3 + 4D_{66}\left(\frac{m}{a}\right)^2 \left(\frac{p_{wi}}{a}\right)\pi^3 - \bar{N}_{22}\left(\frac{p_{wi}}{a}\right)\pi \right] \cdot e^{\beta_{1i}} W_i \sin \alpha \tag{D.14}$$

$$\hat{M} = \sum_{i=1}^{4} \left[D_{12}\left(\frac{m}{a}\right)^2 \pi^2 - D_{22}\left(\frac{p_{wi}}{a}\right)^2 \pi^2 \right] e^{\beta_{1i}} W_i \sin \alpha \tag{D.15}$$

$$\hat{N} = \sum_{i=1}^{4} \left[-A_{12}\left(\frac{m}{a}\right)\pi + A_{22}\left(\frac{p_{ui}}{a}\right) L_{3i}\pi - \bar{N}_{22}\left(\frac{p_{ui}}{a}\right) L_{3i}\pi \right] \cdot e^{\beta_{2i}} U_i \sin \alpha \tag{D.16}$$

$$\hat{T} = \sum_{i=1}^{4} \left[A_{66} \left\{ \left(\frac{p_{ui}}{a} \right) \pi + \left(\frac{m}{a} \right) L_{3i}\, \pi \right\} - \bar{N}_{22} \left(\frac{p_{ui}}{a} \right) \pi \right] \cdot e^{\beta_{2i}} U_i \cos \alpha \qquad (D.17)$$

Putting $y = \pm \frac{b}{2}$ in β_{1i} and β_{2i} of equations (D.1) to (D.3) equations (D.10) to (D.17) yield the buckling displacements and the corresponding forces along the two sides of the flat plate-strip element, when the coupling between bending and stretching is absent.

The subsequent analysis is identical to that in sub-section B.1. Because of the uncoupling between inplane and out-of-plane displacements, the vector W_i in equations (B.22), (B.29), (B.34) and (B.35) becomes $[W_1 \ldots W_4, U_1 \ldots U_4]^T$.

APPENDIX E

UPPER BOUND LOAD P_u

For a chosen m value, a load P_r (for each element making up the structure) is defined in Appendix C as the buckling load of the element when the sides corresponding to the inter-element junction lines are completely restrained. Specified boundary conditions along any external longitudinal (x) side of plate-strip elements are kept unchanged. The smallest of the P_r values is then the upper bound load P_u for the structure. Thus, for each value of m there is a corresponding upper bound load P_u. As a consequence of the beam element axis always coinciding with an inter-element junction line, the above mentioned restraints make it possible to safely ignore these elements from upper bound considerations. Thus, further discussions are limited to plate-strip elements only. Two basic cases considered are:

(1) plate-strip elements clamped along both longitudinal (x) sides;

(2) plate-strip elements clamped along one longitudinal (x) side and with arbitrary restraint conditions along the other side. The latter side corresponds to an external longitudinal (x) side of the structure. It is obvious that when the arbitrary restraints correspond to clamped conditions, such plate-strip elements fall under the category (1) above.

B.1 Plate-Strip Elements with Both Sides Clamped

The analysis given below, for the buckling load P_r of curved plate-strip elements degenerate to the case of flat plate-strip elements in the limit of curvature becoming zero (infinite radius). The onset of buckling in the plate-strip elements with clamped sides is characterized by predominantly out-of-plane displacements. Hence, the basic equations (A.1) and (A.13) to (A.23) are further simplified by dropping the underlined terms. This reduces the numerical complexity and the resulting equations are accurate enough for the upper bound calculations.

As outlined below, the three stability equations (A.13) to (A.16) are uncoupled by the use of the inverse operator, in the manner of Ref. 29 and as further illustrated in Ref. 30. After substituting equations (A.1), (A.5) and (A.6), the above equations are written in terms of buckling displacements u, v and w, as:

$$\bar{L}_1 u + \bar{L}_2 v + \bar{L}_3 w = 0 \tag{E.1}$$

$$\bar{L}_2 u + \bar{L}_4 v + \bar{L}_5 w = 0 \tag{E.2}$$

$$\bar{L}_3 u + \bar{L}_5 v + \bar{L}_6 w = 0 \tag{E.3}$$

where

$$\bar{L}_1 = A_{11}\,(\,)_{,xx} + A_{66}\,(\,)_{,yy}$$

$$\bar{L}_2 = (A_{12} + A_{66})\,(\,)_{,xy}$$

$$\bar{L}_3 = -\left[B_{11}\,(\,)_{,xxx} + (B_{12} + 2B_{66})\,(\,)_{,xyy} + \frac{A_{12}}{R}\,(\,)_{,x}\right]$$

$$\bar{L}_4 = A_{22}\,(\,)_{,yy} + A_{66}\,(\,)_{,xx}$$

$$\bar{L}_5 = -\left[(B_{12} + 2B_{66})\,(\,)_{,xxy} + B_{22}\,(\,)_{,yyy} + \frac{A_{22}}{R}\,(\,)_{,y}\right] \tag{E.4}$$

$$\bar{L}_6 = D_{11}\,(\,)_{,xxxx} + (2D_{12} + 4D_{66})\,(\,)_{,xxyy} + D_{22}\,(\,)_{,yyyy}$$
$$+ 2\frac{B_{12}}{R}\,(\,)_{,xx} + \frac{2B_{22}}{R}\,(\,)_{,yy} + \frac{A_{22}}{R^2}\,w$$
$$+ \bar{N}_{11}\,(\,)_{,xx} + \bar{N}_{22}\,(\,)_{,yy}$$

The $\bar{L}_i$ are linear differential operators and are cummutative. Thus, from equations (E.1) and (E.2) the displacements u and v are expressed in terms of w, as:

$$[(\bar{L}_2)^2 - \bar{L}_1\bar{L}_4]u = [\bar{L}_3\bar{L}_4 - \bar{L}_2\bar{L}_5]w \tag{E.5}$$

$$[(\bar{L}_2)^2 - \bar{L}_1\bar{L}_4]v = [\bar{L}_1\bar{L}_5 - \bar{L}_2\bar{L}_3]w \tag{E.6}$$

A suitable out-of-plane buckling displacement function, satisfying the conditions of zero deflection and zero slope along the sides is:

$$w = \sin\alpha \sum_{n=1}^{\infty} W_n \,(\cos y_{1n} - \cos y_{2n}) \tag{E.7}$$

where

$$y_{1n} = \left[\frac{(n-1)\pi y}{b}\right] \qquad \text{and} \qquad y_{2n} = \left[\frac{(n+1)\pi y}{b}\right] \tag{E.8}$$

The operations indicated on the right side of equations (E.5) and (E.6) result in:

$$(\bar{L}_3\bar{L}_4 - \bar{L}_2\bar{L}_5)\, w = \cos\alpha \left[\sum_n W_n \,(k_{1n} \cos y_{1n} - k_{2n} \cos y_{2n})\right] \tag{E.9}$$

$$(\bar{L}_1\bar{L}_5 - \bar{L}_2\bar{L}_3)\, w = \sin\alpha \left[\sum_n W_n \,(k_{3n} \sin y_{1n} - k_{4n} \sin y_{2n})\right] \tag{E.10}$$

Expressions for the coefficients k_{1n} to k_{4n} though not given here, may be readily derived. From the form of the right sides of the above equations, suitable functions for u and v displacements are chosen as:

$$u = \cos\alpha \left[\sum W_n \,(k_{5n} \cos y_{1n} - k_{6n} \cos y_{2n})\right] \tag{E.11}$$

$$v = \sin\alpha \left[\sum W_n (k_{7n} \sin y_{1n} - k_{8n} \sin y_{2n})\right] \qquad (E.12)$$

where the coefficients k_{5n} to k_{8n} are yet to be determined. Using these equations, the operations indicated by the left side of equations (E.5) and (E.6) yield:

$$\left[(\bar{L}_2)^2 - \bar{L}_1\bar{L}_4\right]u = \cos\alpha \left[\sum W_n (k_{9n}k_{5n} \cos y_{1n} - k_{10n}k_{6n} \cos y_{2n})\right] \qquad (E.13)$$

$$\left[(\bar{L}_2)^2 - \bar{L}_1\bar{L}_4\right]v = \sin\alpha \left[\sum W_n (k_{11n}k_{7n} \sin y_{1n} - k_{12n}k_{8n} \sin y_{2n})\right] \qquad (E.14)$$

The coefficients k_{9n} to k_{12n} may be readily derived. The yet undetermined coefficients k_{5n} to k_{8n} are solved for, by substituting equations (E.9), (E.10), (E.13) and (E.14) in equations (E.5) and (E.6). The functions for the compatible displacements u and v are thus defined in terms of w. They satisfy equations (E.1) and (E.2). The amplitude constants W_n are the only unknowns.

The displacement functions are now substituted in equation (E.3) where the external loading $\bar{N}_{11}$ and $\bar{N}_{22}$ appear in the operator $\bar{L}_6$. The resulting equation is solved for the buckling load using the Galerkin method, Ref. 8. The Galerkin multiplier used is:

$$G_j = \sin\alpha \left[\cos\frac{(j-1)\pi y}{b} - \cos\frac{(j+1)\pi y}{b}\right] \qquad (E.15)$$

Following the method of Ref. 29 results in an infinite set of homogeneous linear equations involving the unknown amplitude constants W_n. As shown therein, these equations are separable into two subsets, one containing only odd values of n and the other containing only even values of n. The buckling load P_r is obtained from the coefficient matrices of these subsets of equations using standard linear eigenvalue solution techniques. The solution by the Galerkin method is known to converge rapidly as the number of terms n retained in the displacement functions is increased. The details of the method outlined above, for determining the buckling load P_r of plate-strip elements with both sides clamped, are easily worked out following the procedure of Ref. 28.

Along the two longitudinal (x) sides of the plate-strip elements, the displacement functions of equations (E.7), (E.11) and E.12) satisfy the boundary conditions.

$$w = \left(\theta = \frac{\partial w}{\partial y} \right) = v = N_{12} = 0 \qquad \text{(E.16)}$$

This shows that there is no restraint to the freedom corresponding to u displacement. As discussed previously, the required clamped conditions along the two sides of the plate-strip elements correspond to complete restraint to all the four degrees of freedom along inter-element junction lines. However, the P_r values for the boundary conditions in equation (E.16) is satisfactory for the purposes of estimating the upper bound load P_u.

E.2 Plate-Strip Elements With One Side Clamped and Other Side Arbitrarily Supported

Plate-strip elements with arbitrary restraint conditions along one external longitudinal (x) side and with clamped conditions along the other side corresponding to an inter-element junction line are now considered. In this case, the choice of buckling displacement function satisfying all boundary conditions, becomes difficult. Thus the method of sub-section E.1 cannot be directly used to determine the buckling load P_r of such plate-strip elements.

Consider the plate-strip element ABCD shown in Figure 18. Using local co-ordinates only (i.e., ϕ_A and ϕ_B given by equations (5.31) and (B.32) are zero), equations similar to (B.36) and (B.37) are readily derived as:

$$\begin{Bmatrix} f_{AD} \\ f_{BC} \end{Bmatrix} = \begin{bmatrix} s_{11} & s_{12} \\ s_{21} & s_{22} \end{bmatrix} \begin{Bmatrix} d_{AD} \\ d_{BC} \end{Bmatrix} \qquad \text{(E.17)}$$

Assume that the side AB has arbitrary restraints specified by the spring stiffness matrix k_A identical to k_o in equation (B.39). The clamped conditions along the side BC corresponds to a similar spring stiffness matrix k_B, whose elements are theoretically infinite. The buckling equation for the plate-strip element is then:

$$\begin{Bmatrix} f_{AD} \\ f_{BC} \end{Bmatrix} = \begin{bmatrix} (s_{11} + k_A) & s_{12} \\ s_{21} & (s_{22} + k_B) \end{bmatrix} \begin{Bmatrix} d_{AD} \\ d_{BC} \end{Bmatrix} = 0 \qquad \text{(E.18)}$$

Since the side BC is completely restrained, the above equation reduces to:

$$[s_{11} + k_A] \{d_{AD}\} = 0 \qquad \text{(E.19)}$$

The buckling load P_r of the plate-strip element under consideration then corresponds to the smallest root of the determinantal equation:

$$\left| (s_{11} + k_A) \right| = 0 \qquad \text{(E.20)}$$

Equation (E.20) being identical to equation (B.59), the algorithm outlined in Appendix C is readily applicable. An upper bound load to the solution of equation (E.20) is obtained by using the Galerkin method discussed in sub-section E.1.

E.3 Upper Bound Load P_u

For each plate-strip element in the structure under consideration and for a chosen m value, a buckling load P_r is evaluated applying the methods discussed in sub-sections E.1 and E.2. The smallest of the P_r values is then the upper bound load P_u. Each value of m has a corresponding upper bound load.

Initially the procedure described might appear rather tedious. However, in actual structures it will not be necessary to evaluate P_r values for all plate-strip elements. Some elements can be eliminated from consideration due to their repetition in the structure, while others can be eliminated because of physical considerations.

APPENDIX F

CONVERSION OF U.S. CUSTOMARY UNITS TO SI UNITS

The International System of Units (SI) was adopted by the Eleventh General Conference on Weights and Measures, Paris, October 1960, in Resolution No. 12. (See ref. 31.) Conversion factors for the units used herein are given in the following tables:

Physical quantity	U.S. Customary Unit	Conversion factor (*)	SI Unit (**)
Area	in^2	6.452×10^{-4}	square meters (m^2)
Force	kip = 1000 lbf	4.448×10^{3}	newtons (N)
Length	in.	2.54×10^{-2}	meters (m)
Moduli and stress	ksi = 1000 lbf/in^2	6.895×10^{6}	newtons per square meter (N/m^2)
Stress resultant	lbf/in.	175.1	newtons per meter (N/m)

* Multiply value given in U.S. Customary Unit by conversion factor to obtain equivalent value in SI Unit.

** Prefixes to indicate multiple of units are as follows:

Prefix	Multiple
milli(m)	10^{-3}
centi(c)	10^{-2}
kilo(k)	10^{3}
giga(G)	10^{9}

REFERENCES

1. Viswanathan, A. V., Soong, Tsai-Chen, Miller, R. E. Jr.: Buckling Analysis for Axially Compressed Flat Plates, Structural Sections and Stiffened Plates Reinforced with Laminated Composites. NASA CR-1887, November 1971. Also Int. J. of Solids and Structures, Vol. 8, 1972, pp. 347-367.

2. Viswanathan, A. V., Soong, T. C., Miller, R. E.: Compressive Buckling Analysis and Design of Stiffened Flat Plates with Multilayered Composite Reinforcement. Computers & Structures, vol. 3, 1973, pp. 281-297.

3. Giles, Gary L.: Structural Efficiencies of Five Compression Panels with Curved Elements. NASA TN D-6479, December 1971.

4. Buchwald, V. T.: Some Problems of Thin Circular Cylindrical Shells I - The Equations. J. of Math and Physics, Vol. 46, Sept. 1967, pp. 237-252.

5. Cheng, Shun: Accurate Fourth Order Equations for Circular Cylindrical Shells, J. of the Engr. Mech. Div., Proc. A.S.C.E., June 1972, pp. 641-656.

6. Novozhilov, V. V.: Thin Shell Theory, P. Noordhoff Ltd., Netherlands, 1964.

7. Wittrick, W. H., Williams, F. W.: A General Algorithm for Computing Natural Frequencies of Elastic Structures. Quarterly J. of Mech. and App. Maths, Vol. 24, Part 3, August 1971, pp. 263-284.

8. Duncan, W. J.: Principles of the Galerkin Method, R&M No. 1848, Aeronautical Research Committee, Sept. 1938.

9. Tripp, Leonard L., Tamekuni, M., Viswanathan, A. V.: A computer Program for Instability Analysis of Biaxially Loaded Composite Stiffened Panels and Other Structures: Users Manual for "BUCLASP2" NASA CR-112226, 1973.

10. Timoshenko, S. P., Gere, J. M.: Theory of Elastic Stability, 2nd ed., McGraw-Hill, 1961.

11. Card, M. F.: The Sensitivity of Buckling of Axially Compressed Fiber-Reinforced Cylindrical Shells to Small Geometric Imperfections. Ph.D Dissertation, Virginia Polytechnic Institute, Blacksburg, Virginia, Dept. of Engineering Mechanics. June 1969.

12. Bushnell, David: Stress, Stability and Vibration of Complex Shells of Revolution: Analysis and User's Manual for "BOSOR3". SAMSO TR-69-375, Space and Missile Systems Organization, September 1969.

13. Bushnell, David: Analysis of Ring-Stiffened Shells of Revolution Under Combined Thermal and Mechanical Loading. AIAA Journal, Vol. 9, No. 3, March 1971, pp. 401-410.

14. Williams, F. W., Wittrick, W. H.: Numerical Results for the Initial Buckling of Some Stiffened Panels in Compression. The Aeronautical Quarterly, Vol. 23, Feb. 1972, pp. 24-40.

15. Pride, R. A. Royster, D. M., Gardner, J. E.: Influence of Various Fabrication Methods on the Compressive Strength of Titanium Skin Stringer Panels. NASA TN D-5389, Aug. 1969.

16. Herring, H. W., Carri, R. L., Webster, R. C.: Compressive Behaviour of Titanium Alloy Skin Stiffener Specimens Selectively Reinforced With Boron - Aluminum Composite, NASA TN D-6548, Nov. 1971.

17. Wilkinson, J. H.: The Algebraic Eigenvalue Problem, Clarendon Press, 1965.

18. Wilkinson, J. W., Reinsch, C.: Handbook for Automatic Computation - Vol. 2: Linear Algebra, Chief editor: F. L. Bauer, Springer-Verlag, 1971.

19. Wittrick, W. H.: A Unified Approach to the Initial Buckling of Stiffened Panels in Compression. The Aeronautical Quarterly, Vol. 19, August 1968, pp. 265-283.

20. Ashton, J. E., Halpin, J. C., Petit, P. E.: Primer on Composite Materials: Analysis, Progress in Material Sciences, Vol. 3, Technomic Publication, 1969.

21. Kempner, Joseph: Unified Thin Shell Theory, PIBAL Report 566, Dept. of Aero. Engg. and App. Mech., Polytechnic Institute of Brooklyn, March 1960.

22. Novozhilov, V. V.: Foundations of the Nonlinear Theory of Elasticity, Graylock Press, 1953.

23. Ramberg, W., Levy, S.: Instability of Extrusions Under Compressive Loads. J. of Aero Sc., Oct. 1945.

24. Argyris, J. H., Dunne, P. C.: Structural Principles and Data, Edited by D.M.A. Legget and M. Langley, Pitman Press, 1934.

25. Roark, R. J.: Formulas for Stresses and Strains, 4th ed., McGraw-Hill, 1965.

26. Lord Rayleigh: The Theory of Sound, Vol. I, Section 92a, pp. 119, Dover Publications, 1945.

27. Gagnon, Claude R.: Generalized Eigenproblem for Large Matrices with a Repeated Block Structure. Internal Report MA-189, Numerical Analysis Staff, Boeing Computer Services, Seattle, July 1970.

28. Lu, Paul: Equation Solver and Generalized Eigenproblem for large Symmetric Matrices with a Special Block Structure. Internal Report MA-237, Numerical Analysis Staff, Boeing Computer Services, Seattle, April 1971.

29. Batdorf, S. B.; A Simplified Method of Elastic Stability Analysis for Thin Cylindrical Shells, NACA Tech. Report No. 874, 1947.

30. Martin, R. E., Drew, D. D.: On the Simplification of the Equations for the Stability Analysis of Anisotropic Cylindrical Shells. SIAM J. of App. Maths., Vol. 18, No. 4, June 1970, pp. 776-782.

31. Mechtly, E. A.: The International System of Units - Physical Constants and Conversion Factors (Revised). NASA SP-7012, 1969.

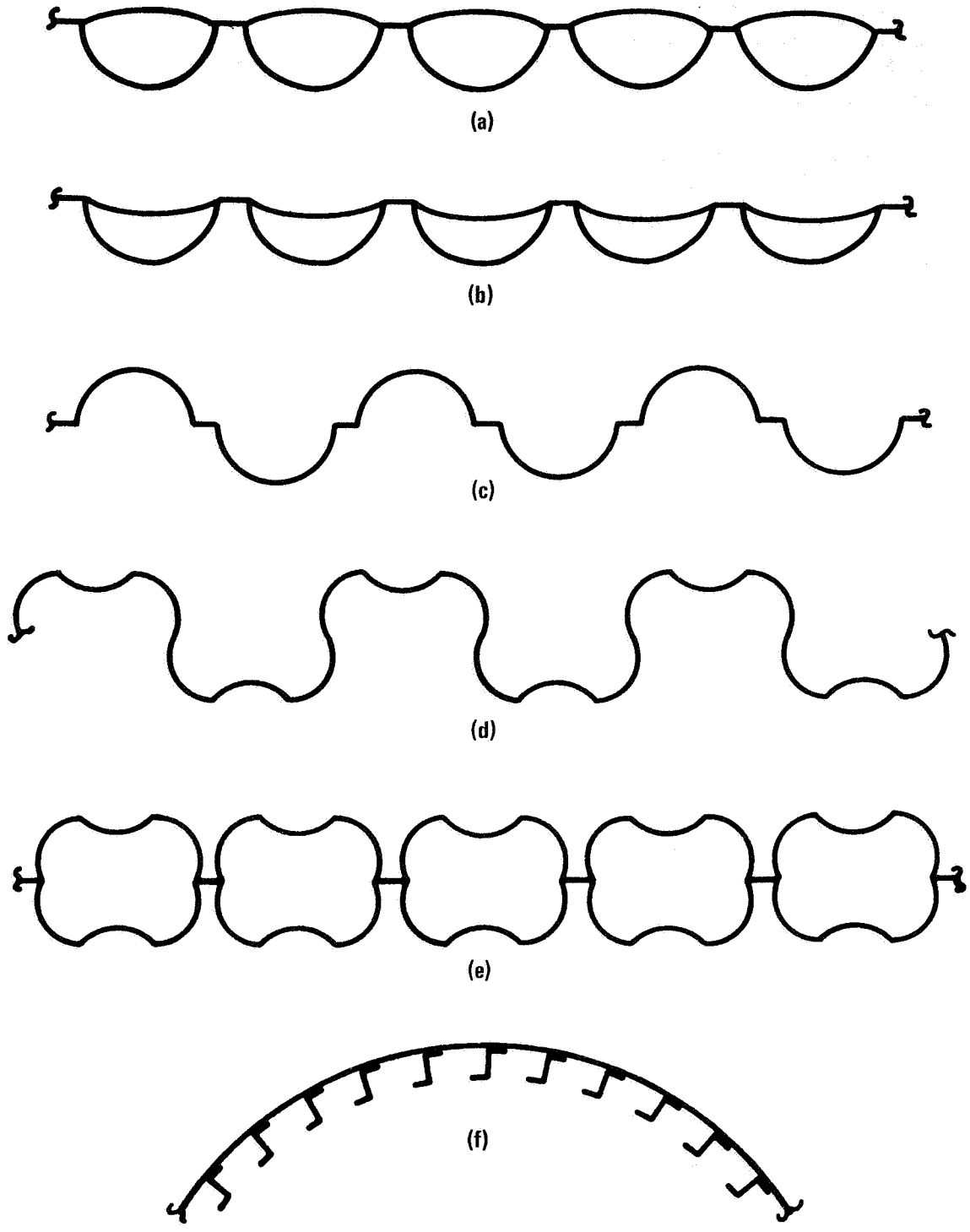

Figure 1.—Panels With Curved Parts

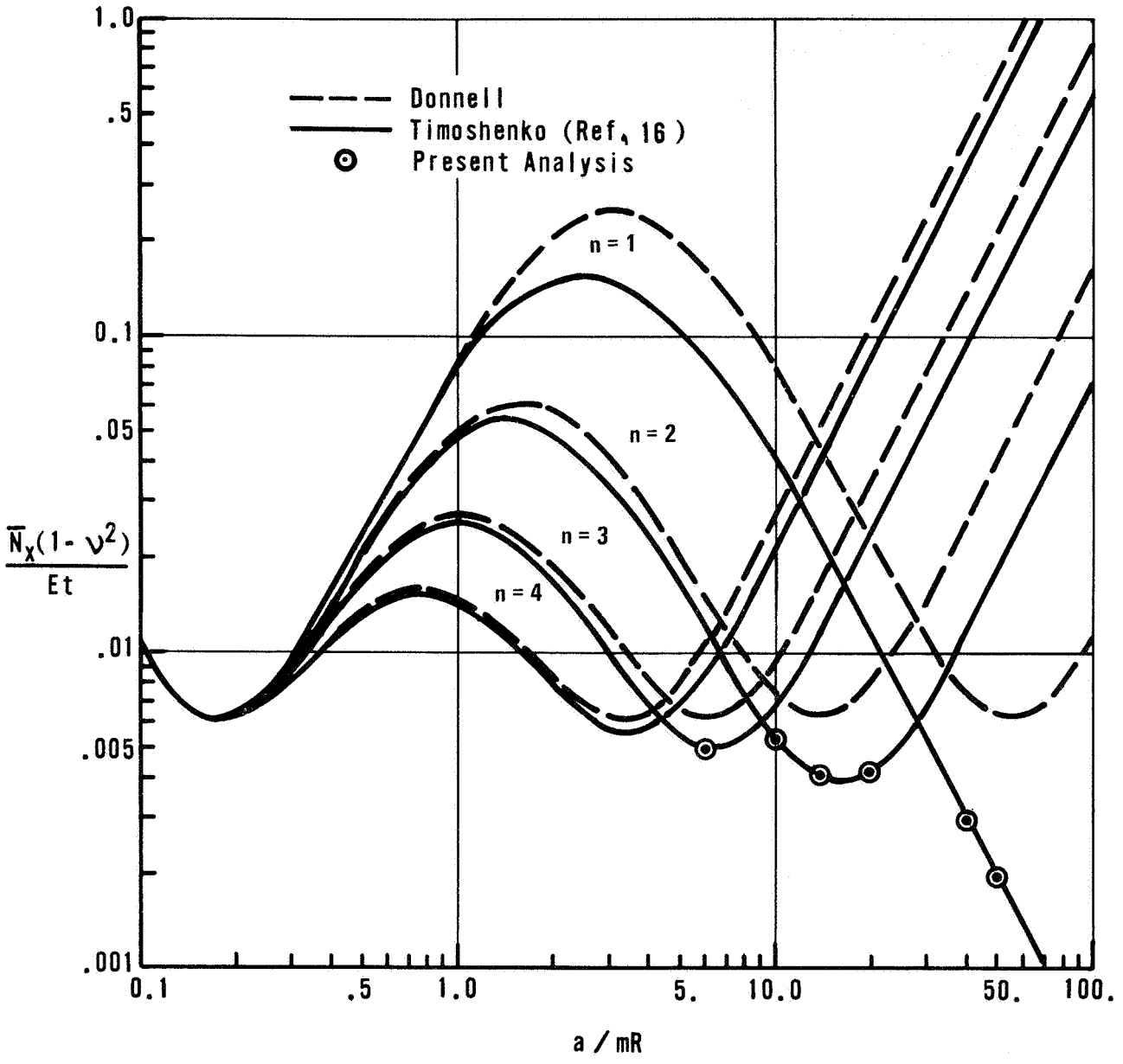

Figure 2.–Buckling of Isotropic Cylinders

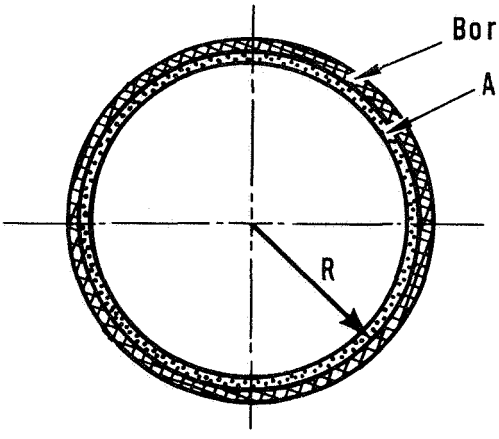

t_{al} = 0.05 inches

$t_{b/e}$ = 0.05 inches

Radius, R = 9.95 inches

Length = 7.0 inches

MATERIAL PROPERTIES

Aluminum:

$E_{11} = E_{22} = 10.5 \times 10^6$ lbs/in^2

$G_{12} = 4.04 \times 10^6$ lbs/in^2

$\nu_{12} = 0.3$

Boron Epoxy:

Fiber Angle	$E_{11} \times 10^{-6}$ lbs/in^2	$E_{22} \times 10^{-6}$ lbs/in^2	ν_{12}	$G_{12} \times 10^{-6}$ lbs/in^2
0	30.250	2.030	0.346	0.525
15	23.800	1.900	1.179	2.339
30	7.762	1.608	1.655	5.967
45	1.977	1.977	0.884	7.782
60	1.608	7.762	0.343	5.967
75	1.900	23.800	0.094	2.339
90	2.030	30.250	0.023	0.525

(Note: E_{11} is the modulus in the direction of cylinder axis)

Figure 3.–Fiber Reinforced Cylindrical Shells (1 of 2)

RESULTS:

Fiber Angle	m	Ref. 22		Present Analysis*		Present Analysis	
		Minimum Buckling Load $\bar{N}_{11}$ lb/in	n	Minimum Buckling Load $\bar{N}_{11}$ lb/in	n**	Minimum Buckling Load $\bar{N}_{11}$ lb/in	n**
0	2	4881	9	4884	9	4853	9
15	3	5144	5	5145	5	5137	5
30	3	5625	3	5631	3	5624	3
45	4	6418	0	6418	0	6414	0
60	1	5953	7	5955	7	5696	7
75	1	5183	7	5183	7	4950	7
90	2	4883	9	4883	9	4734 (m = 1)	9

* Buckling load, when the underlined terms in equations (4.1) and (4.13) to (4.23) are suppressed

** n, the circumferential wave number determined from the buckling mode shape plot

Figure 3.–Fiber Reinforced Cylindrical Shells (2 of 2)

Material Properties: $E_{11} = E_{22} = 10.3 \times 10^6$ lbs/in^2

$G_{12} = 3.87 \times 10^6$ lbs/in^2

$\nu_{12} = 0.33$

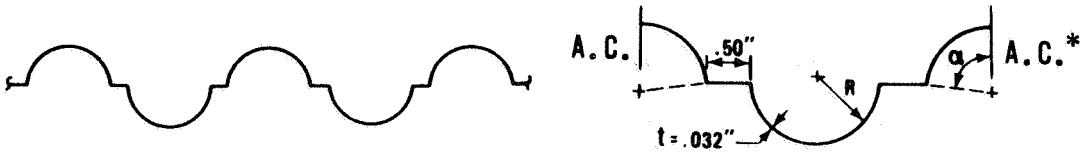

Panel 1: $R = 1.36''$; $\alpha = 82.5^\circ$

Panel 2: $R = 1.20''$; $\alpha = 85^\circ$

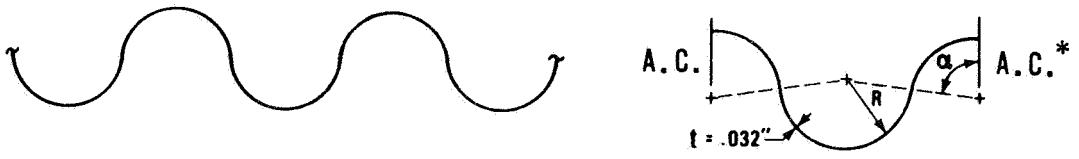

Panel 3: $R = 1.36''$; $\alpha = 82.5^\circ$

Panel 4: $R = 1.20''$; $\alpha = 85^\circ$

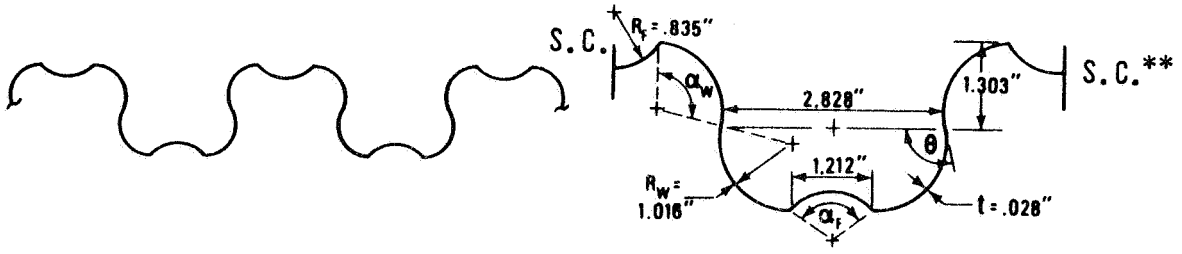

Panel 5: $\alpha_W = 97.92^\circ$; $\alpha_F = 93.02^\circ$; $\theta = 107.2^\circ$

* A.C.	Antisymmetric boundary conditions
** S.C.	Symmetric boundary conditions

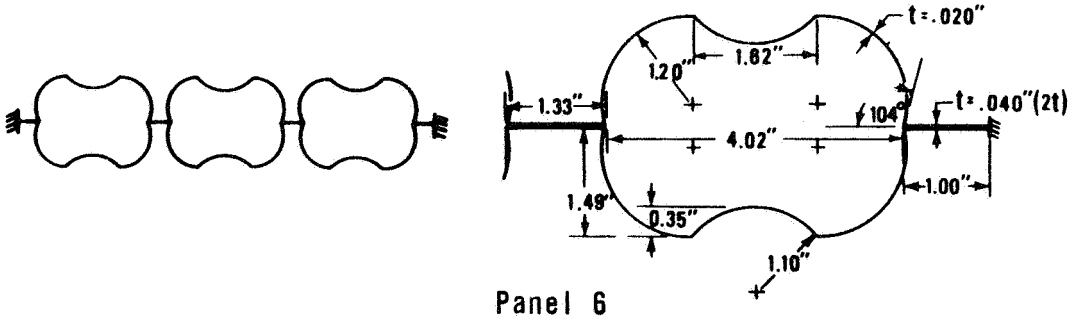

Panel 6

Figure 4.—Advanced Structural Panels

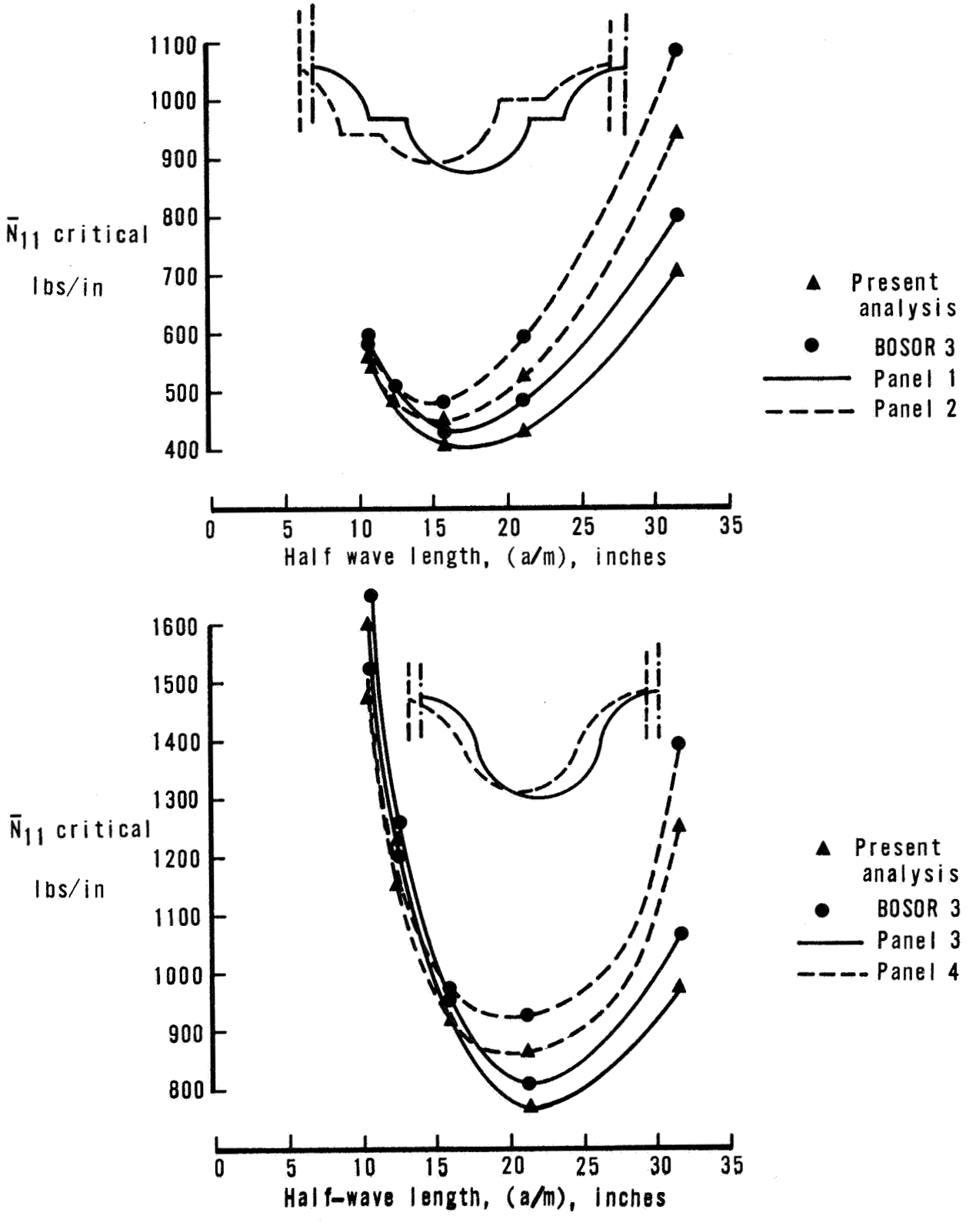

Figure 5.– Results for Advanced Structural Panels (1 of 2)

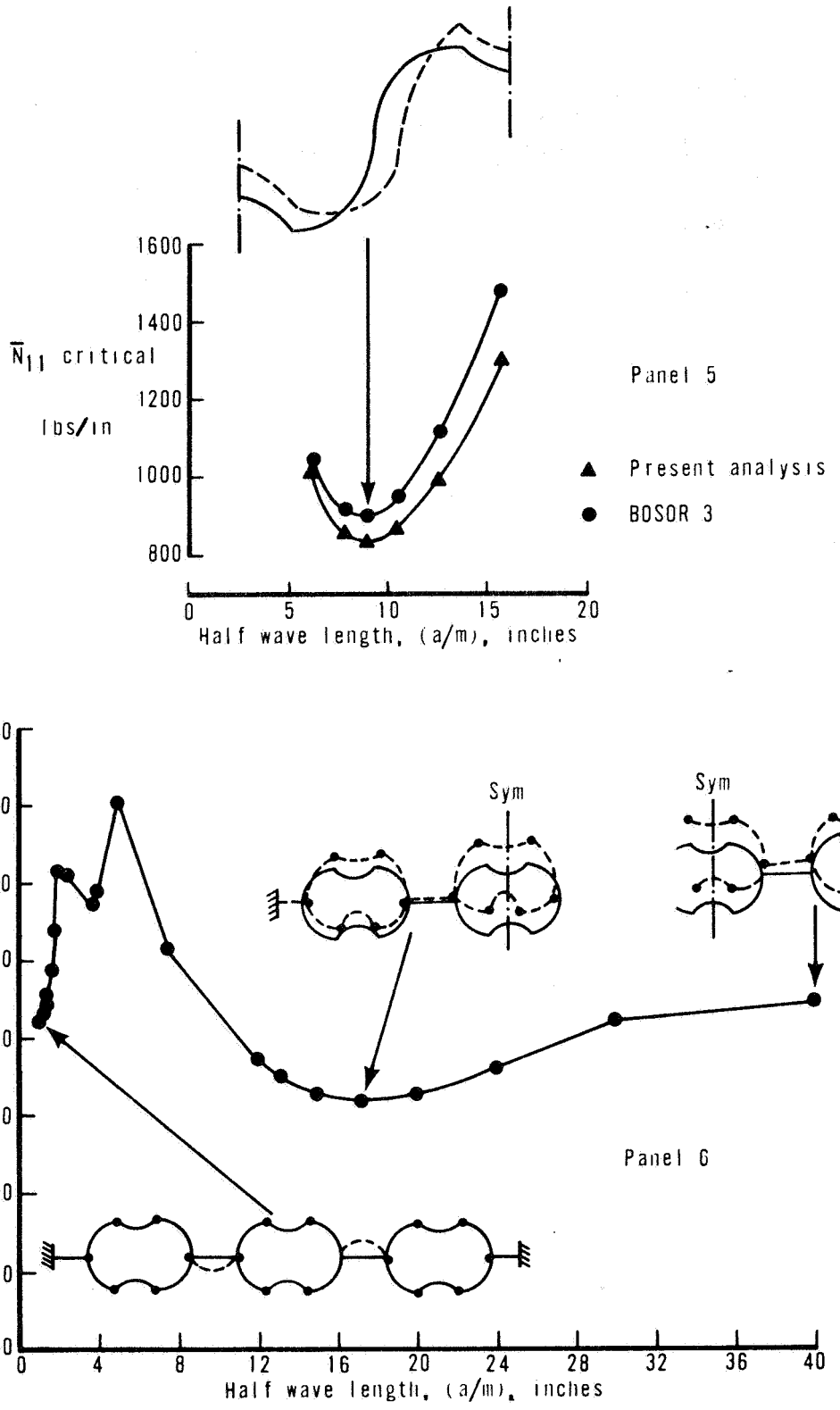

Figure 5.—Results for Advanced Structural Panels (2 of 2)

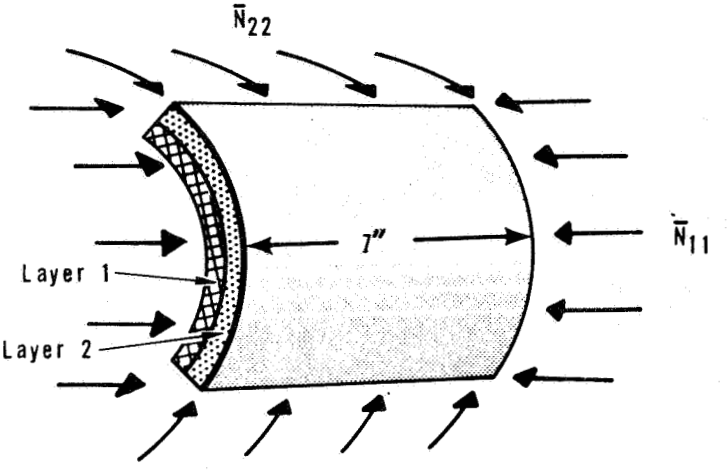

All edges simply supported
Mean radius = 10 inches
Mid-plane chord length = 10 inches
$t_1 = t_2$ = 0.05 inches

Material Properties

	$E_{11} \times 10^{-6}$ lbs/in^2	$E_{22} \times 10^{-6}$ lbs/in^2	$G_{12} \times 10^{-6}$ lbs/in^2	ν_{12}
Layer 1	10.5	10.5	4.04	0.3
Layer 2	30.25	2.03	0.525	0.346

Figure 6.–Biaxially Loaded Laminated Curved Plate

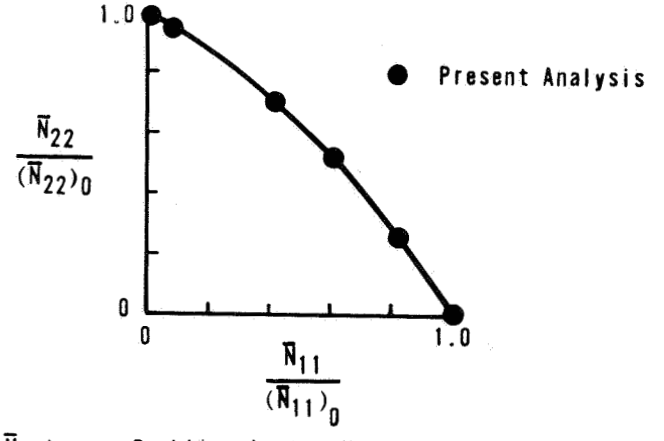

$(\bar{N}_{11})_0$, $(\bar{N}_{22})_0$ — Buckling loads (lbs/in) for individual unidirectional loading

Figure 7.–Results for Biaxially Loaded Laminated Curved Plate (All Edges Simply Supported)

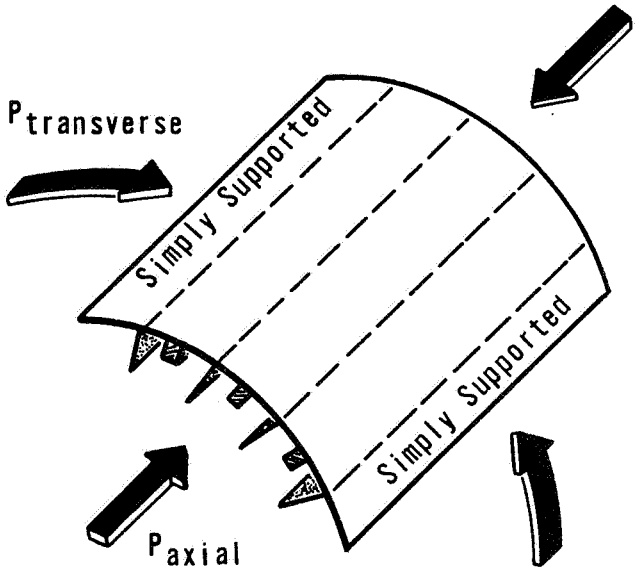

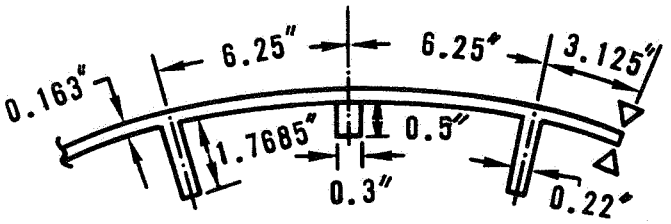

Skin mid-plane radius = 198 inches
Panel length = 50 inches
$P_{transverse}$ = 10,000 lbs (Constant)

Material Properties

Element	$E_{11} \times 10^{-6}$ lbs/in^2	$E_{22} \times 10^{-6}$ lbs/in^2	$G_{12} \times 10^{-6}$ lbs/in^2	$G_{23} \times 10^{-6}$ lbs/in^2	ν_{12}
Plate	10.5	10.5	3.975	—	0.32
Beam	30.0	—	—	0.8	—

Figure 8.—Biaxially Loaded Stiffened Panel

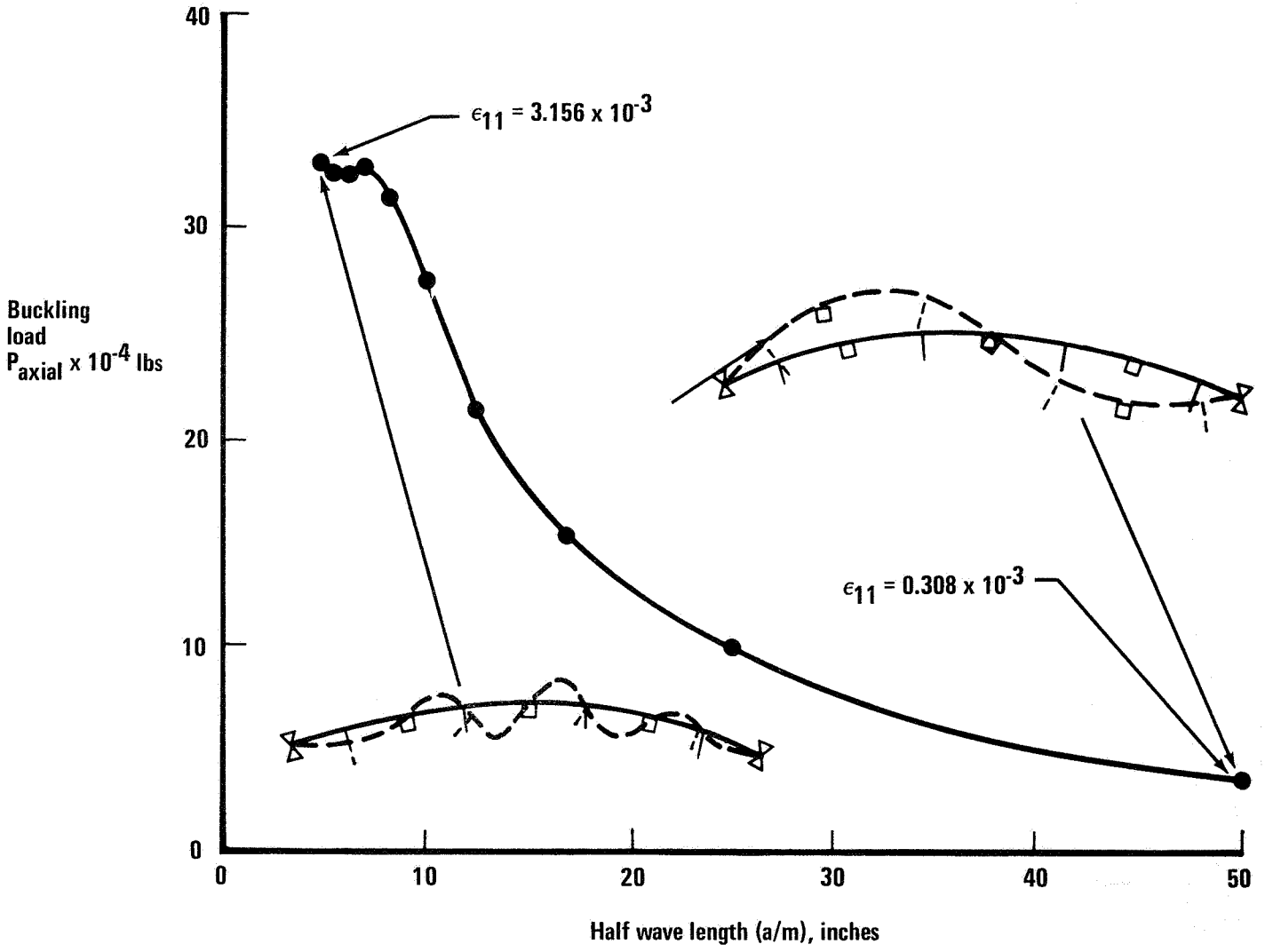

Figure 9.–Results for Biaxially Loaded Stiffened Panel

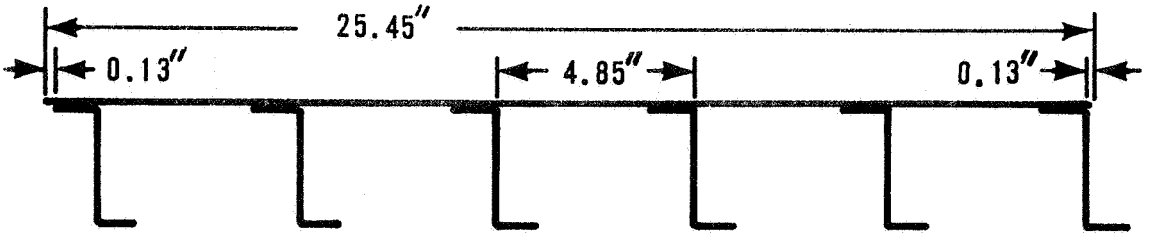

Panel Length = 17.1 inches

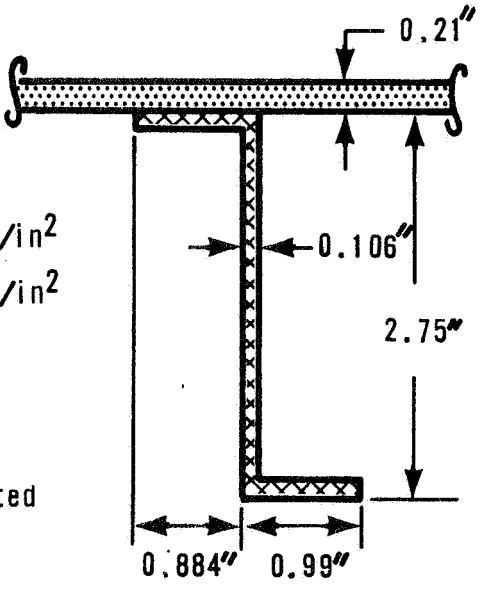

Material Properties

$E_{11} = E_{22}$ = 10.2×10^6 lbs/in^2

G_{12} = 3.92×10^6 lbs/in^2

ν_{12} = 0.3

Panel sides are simply supported

Results

Minimum Buckling Stress (m = 1) = 60,700 lbs/in^2

Buckling Strain = 5.957×10^{-3} in/in

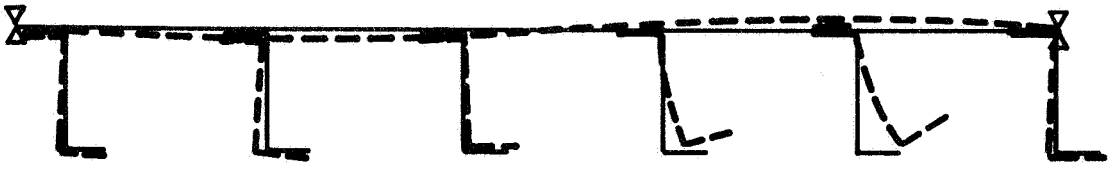

Buckling Mode Shape

Figure 10.—Zee Stiffened Panel

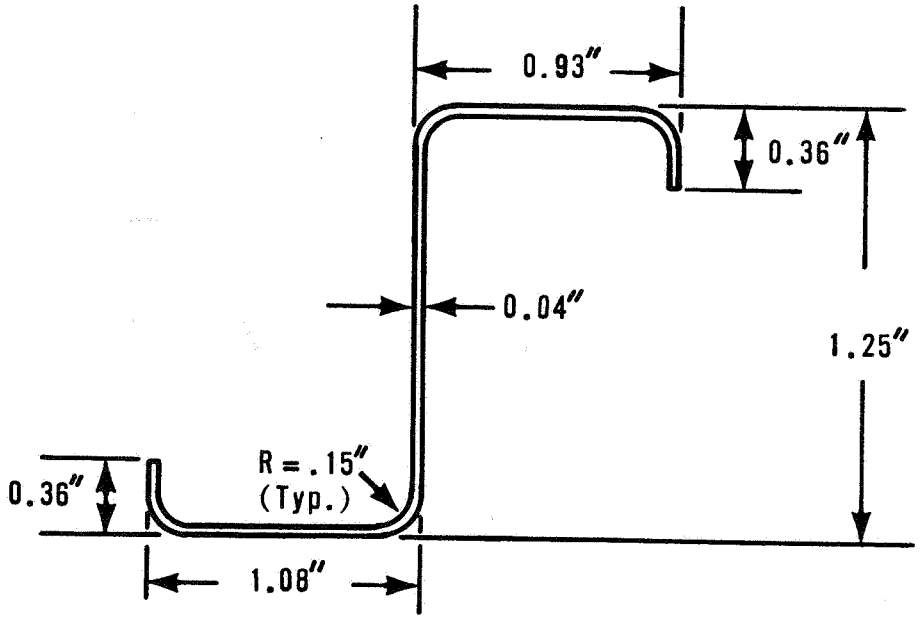

Material Properties

$E_{11} = E_{22} = 16.2 \times 10^6$

$G_{12} = 6.23 \times 10^6$

$\nu_{12} = 0.3$

Length = 3.0 inches

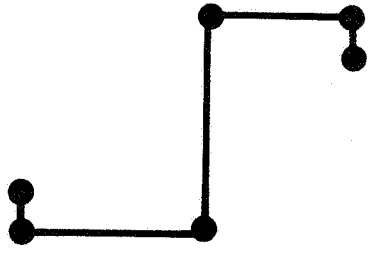

Idealization No. (1)

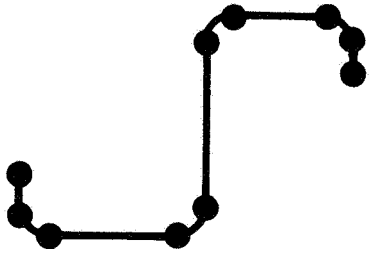

Idealization No. (2)

Figure 11.–Formed Zee Section

m	σ_{cr} = Buckling Stress (kips/in^2)		$\frac{\sigma_{cr}\,②}{\sigma_{cr}\,①}$
	Idealization No. ①	Idealization No. ②	
2	85.0	98.0	1.15
3	78.1	93.0	1.19
4	88.4	104.3	1.18

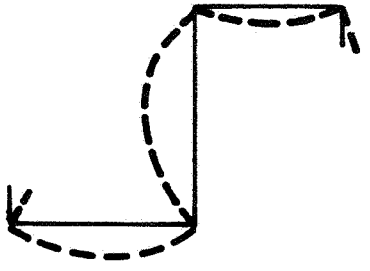

Idealization No. ①

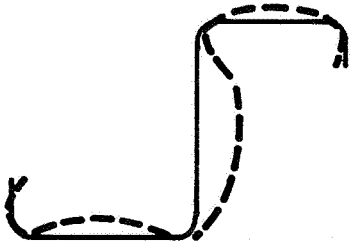

Idealization No. ②

Figure 12.—Results for Formed Zee Section

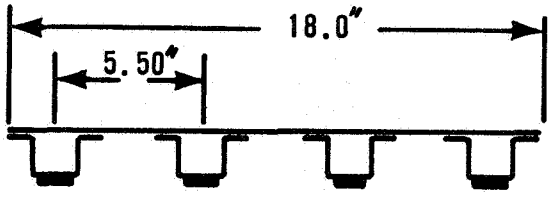

Panel length = 40 inches

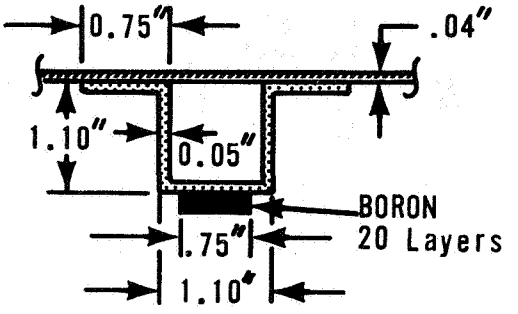

Material Properties

Material	$E_{11} \times 10^{-6}$ lbs/in^2	$E_{22} \times 10^{-6}$ lbs/in^2	$G_{12} \times 10^{-6}$ lbs/in^2	ν_{12}
Titanium	16.4	16.4	6.2	0.3
Boron Fiber Composite	29.117	2.341	0.75	0.2467

(a) Panel Geometry and Material Properties

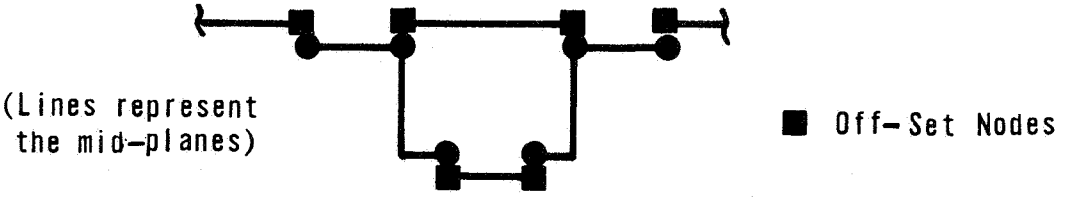

(b) Idealization Showing Offsets

m	Panel Buckling Load (lbs)		Buckling Strain x 10^3 (in/in)	
	With Offsets	Without Offsets	With Offsets	Without Offsets
1	64520	55770	1.7035	1.4726
2	209800	183100	5.5403	4.8339

(c) Results

Figure 13.–Effect of Offsets–Hat Stiffened Panel

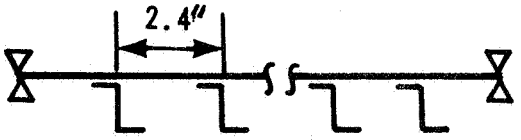

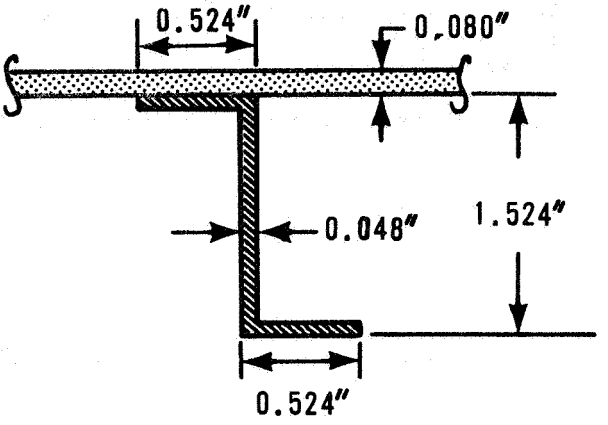

No. of stiffeners = 6

Panel length = 16.0 inches

Material Properties

$E_{11} = E_{22} = 10.0 \times 10^6$ lbs/in^2

$G_{12} = 3.85 \times 10^6$ lbs/in^2

$\nu_{12} = 0.3$

(a) Panel Geometry and Material Properties

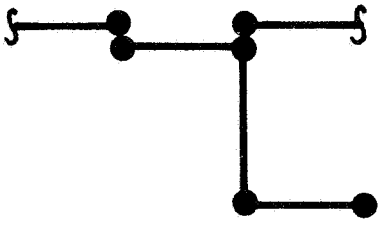

(Lines drawn are through mid-planes)

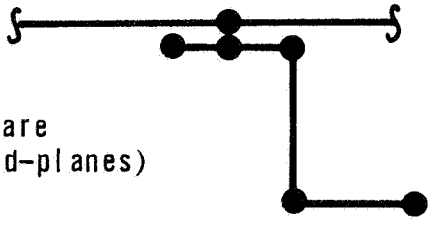

(b) Bonded Stiffener

(c) Riveted Stiffener

RESULTS FOR MINIMUM BUCKLING STRESS

Bonded Panel

$\sigma_{cr} = 49{,}800$ lbs/in^2

$m = 12$

Riveted Panel

$\sigma_{cr} = 38{,}043$ lbs/in^2

$m = 9$

Figure 14.–Bonded and Riveted Connections–Zee Stiffened Panel

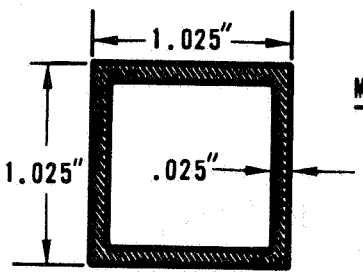

Length = 100.0 inches

Material Properties

$E_{11} = E_{22} = 10.0 \times 10^6$ lbs/in^2

$G_{12} = 3.85 \times 10^6$ lbs/in^2

$\nu_{12} = 0.3$

(a) Square Tube

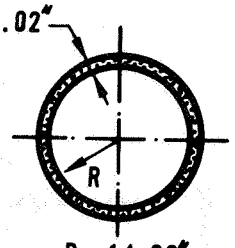

R = 14.99"

Length = 60.0 inches

(b) Thin Walled Cylinder

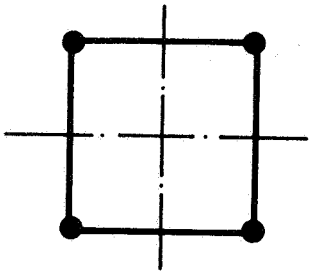

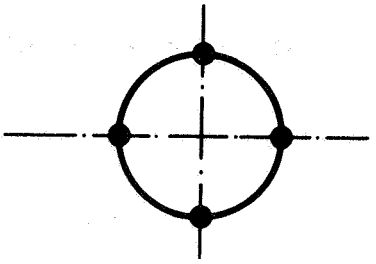

(c) Initial Idealization (Coincident Roots)

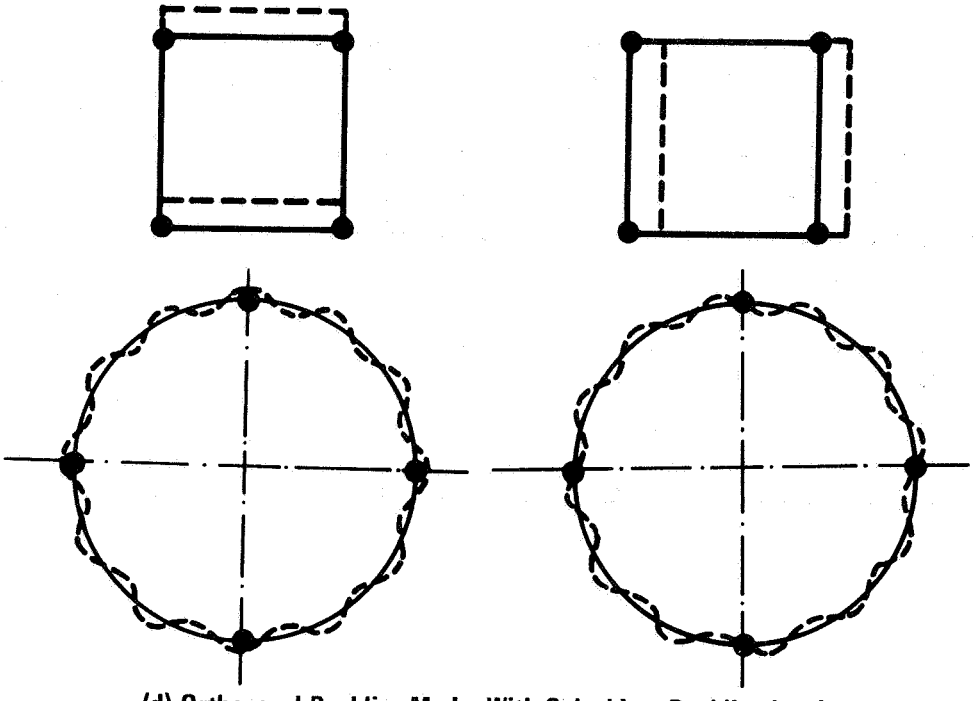

(d) Orthogonal Buckling Modes With Coincident Buckling Loads

Figure 15.–Problems Illustrating Coincident Roots (1 of 2)

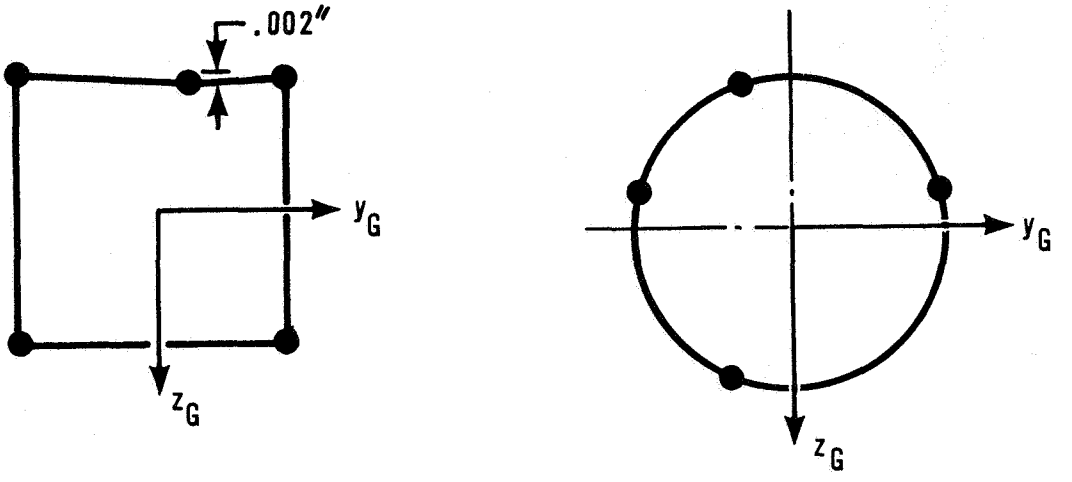

(e) Second Idealization (No Coincident Roots)

EXAMPLE	SQUARE TUBE			THIN WALLED CYLINDER		
IDEALIZATION	Buckling Load $\bar{N}_{11}$ (lbs/in)	m	Change in η Value	Buckling Load $\bar{N}_{11}$ (lbs/in)	m	Change in η Value
Initial	41.0	1	0 to 2	159.2	4	0 to 2
Second	41.0	1	0 to 1	159.2	4	0 to 1
Classical Result	41.1	1	—	159.2	4	—

(f) Results

Figure 15.–Problems Illustrating Coincident Roots (2 of 2)

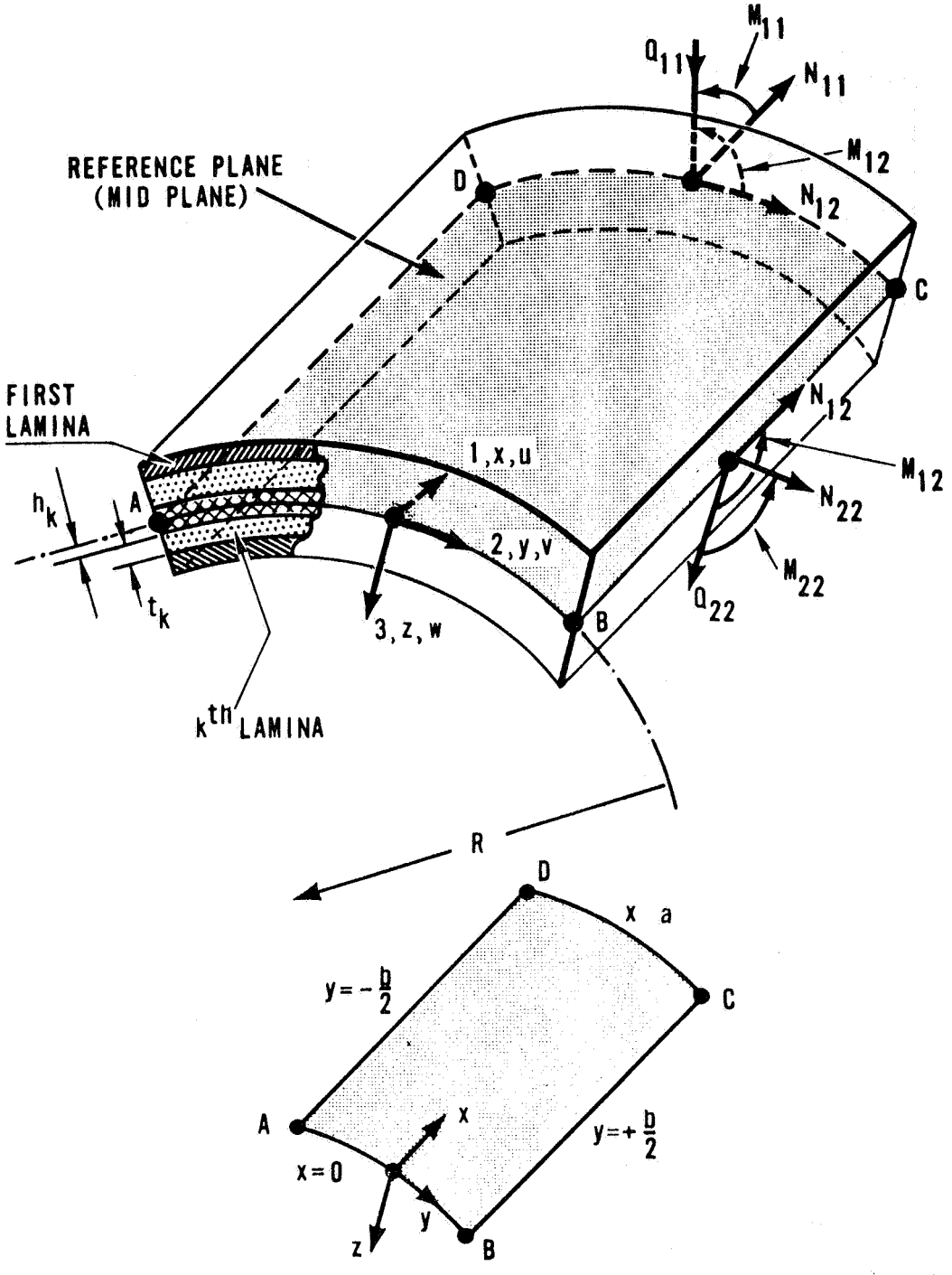

Figure 16.—Laminate Plate—Strip Element

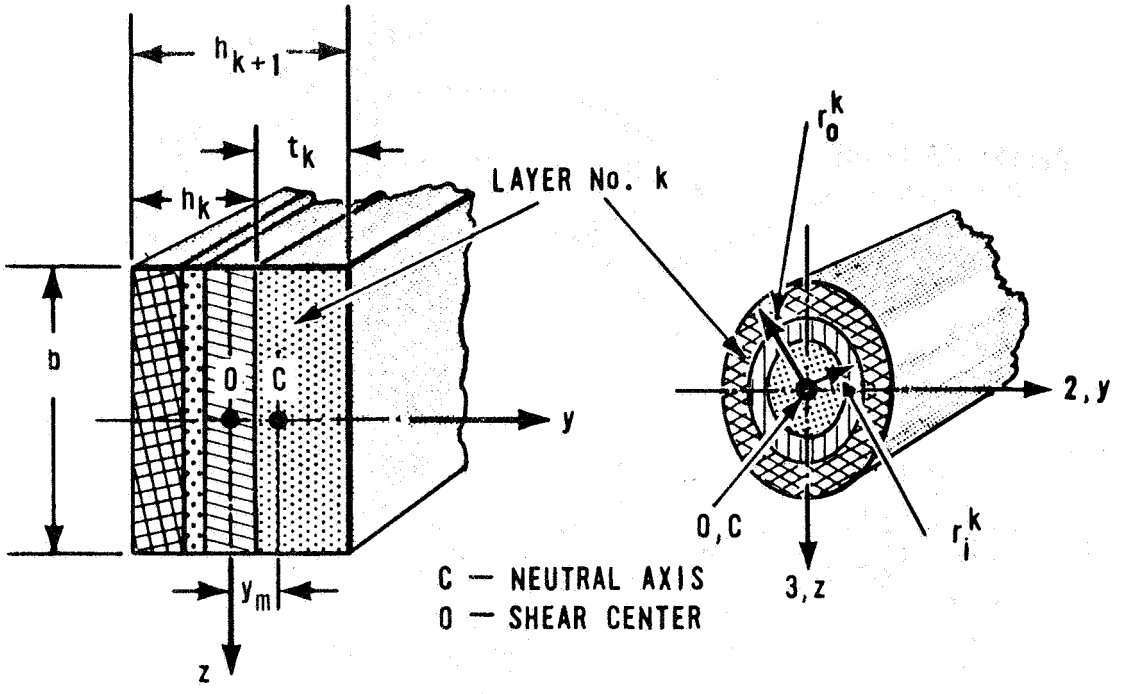

(a) Laminated Rectangular Beam

(b) Laminated Circular Beam

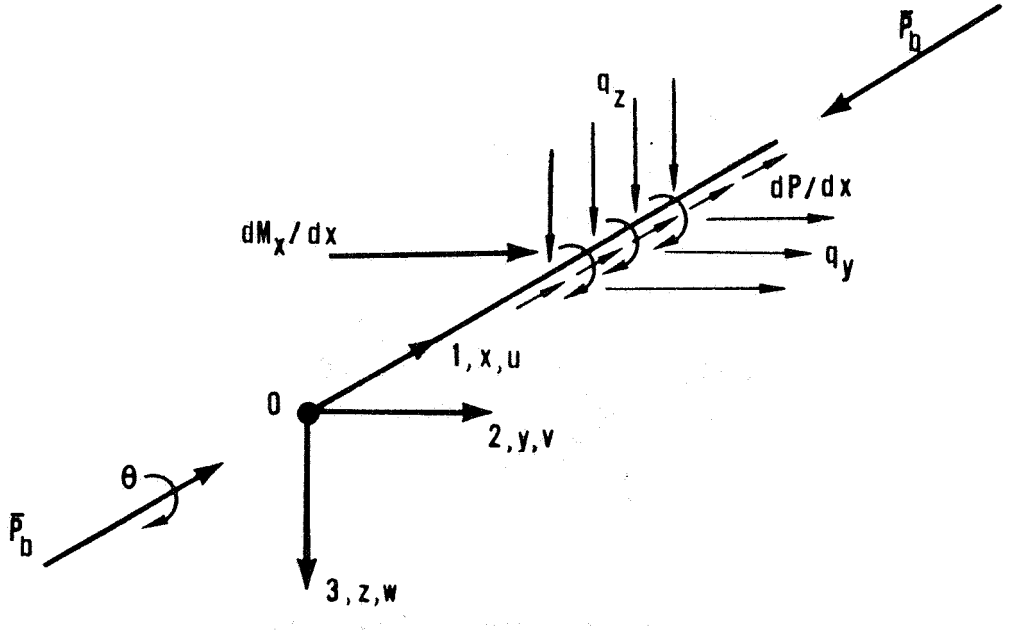

(c) Sign Conversions

Figure 17.—Beam Elements

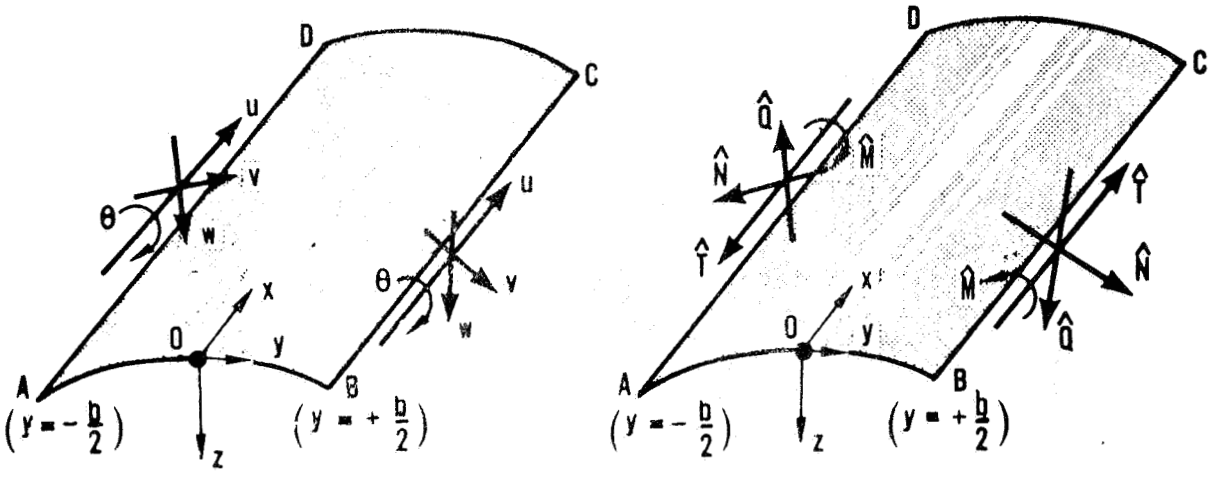

Figure 18.—Displacements and Forces Due to Buckling Along Sides of the Plate-Strip Element

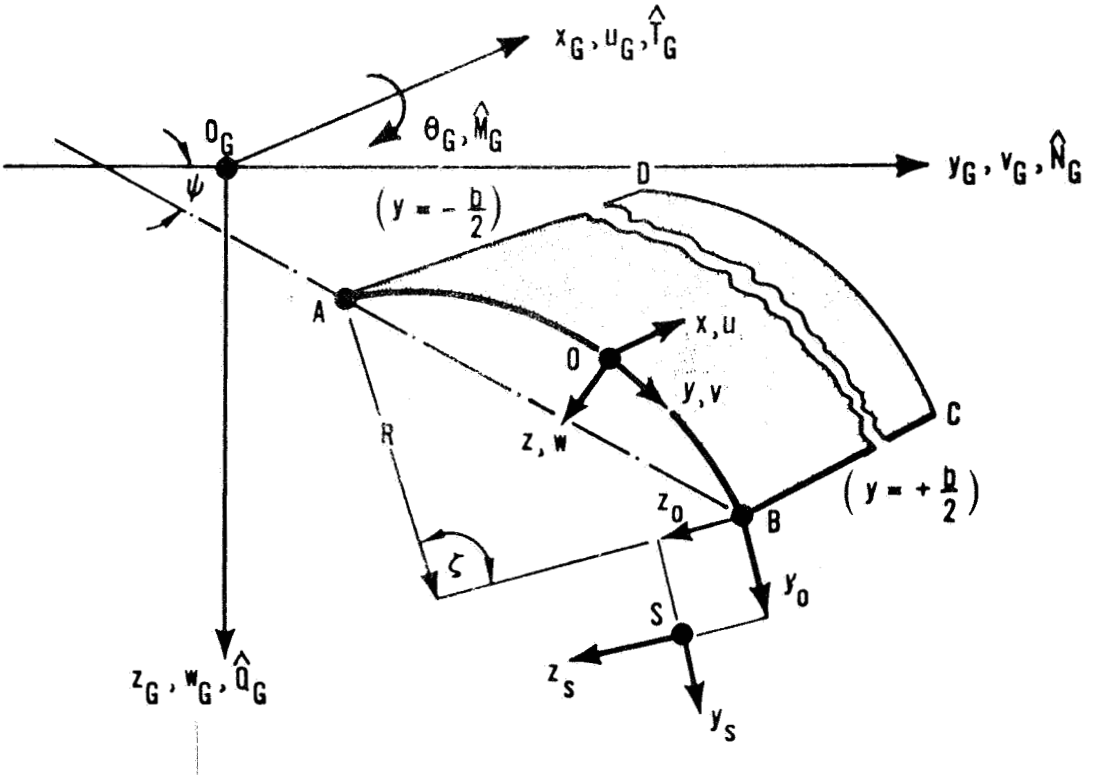

Figure 19.—Offsets and Global Axes for Plate-Strip Element

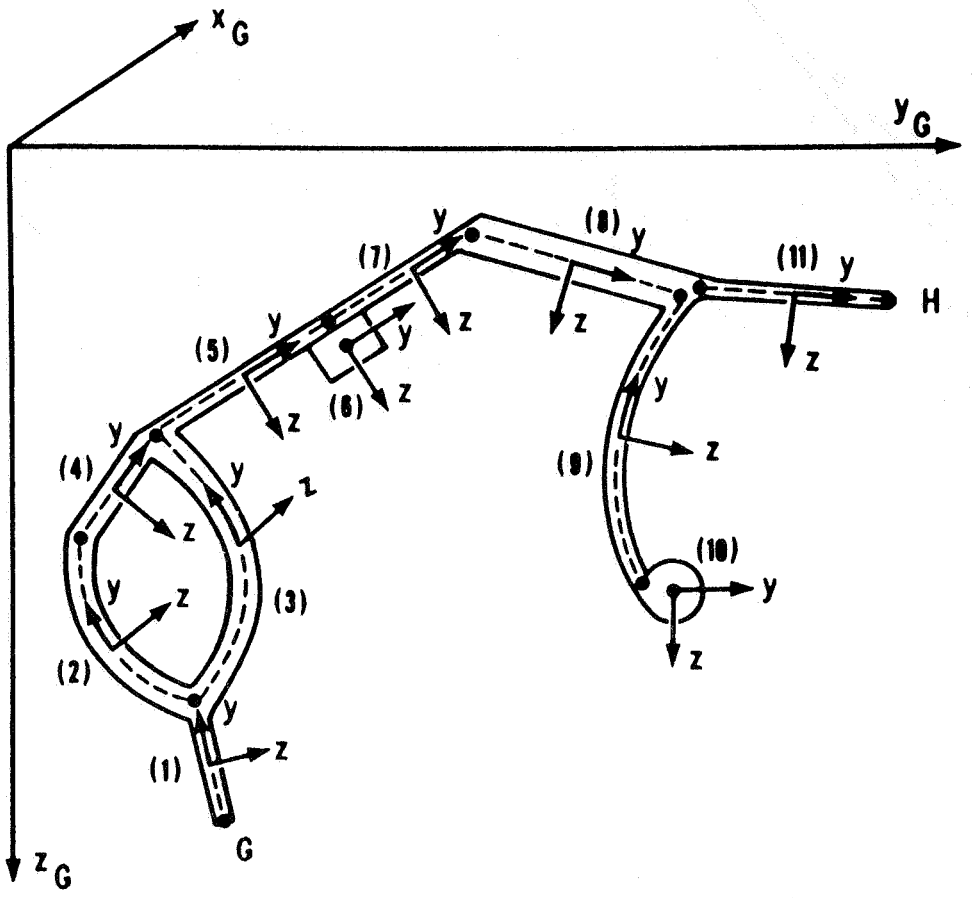

Figure 20.–Idealization of an Arbitrary Structure

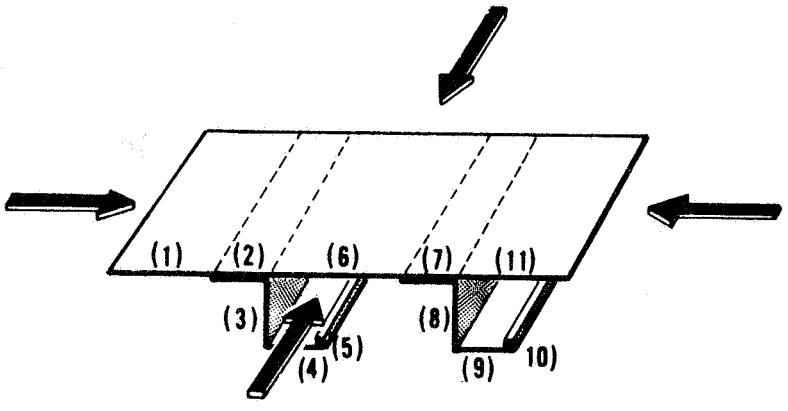

Figure 21.–Typical Stiffened Panel

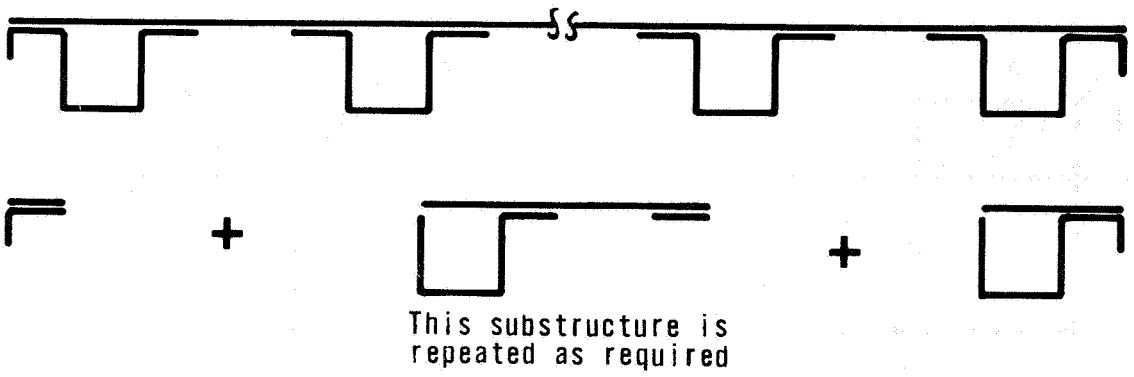

Figure 22.–Example of Open Structure With Repeated Substructures

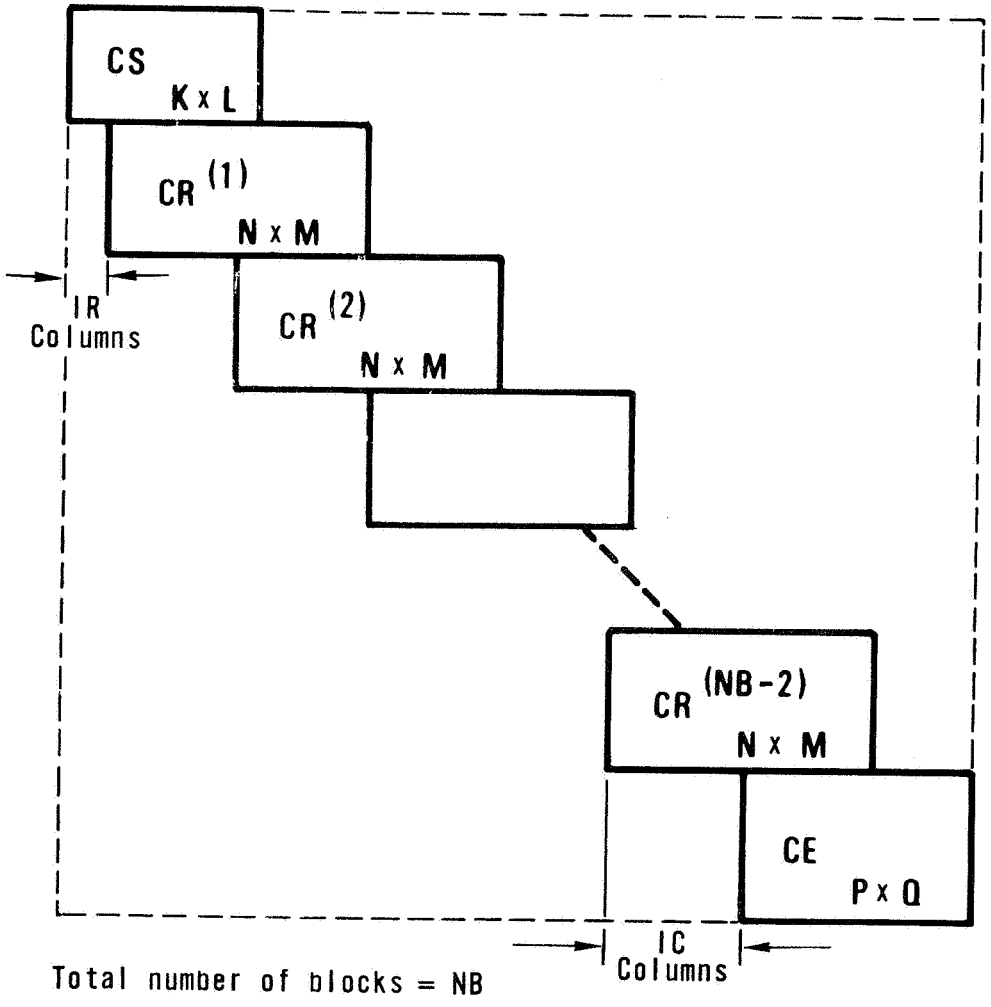

Figure 23.–Stiffness Matrix "S" for Open Structures With Repeated Substructures

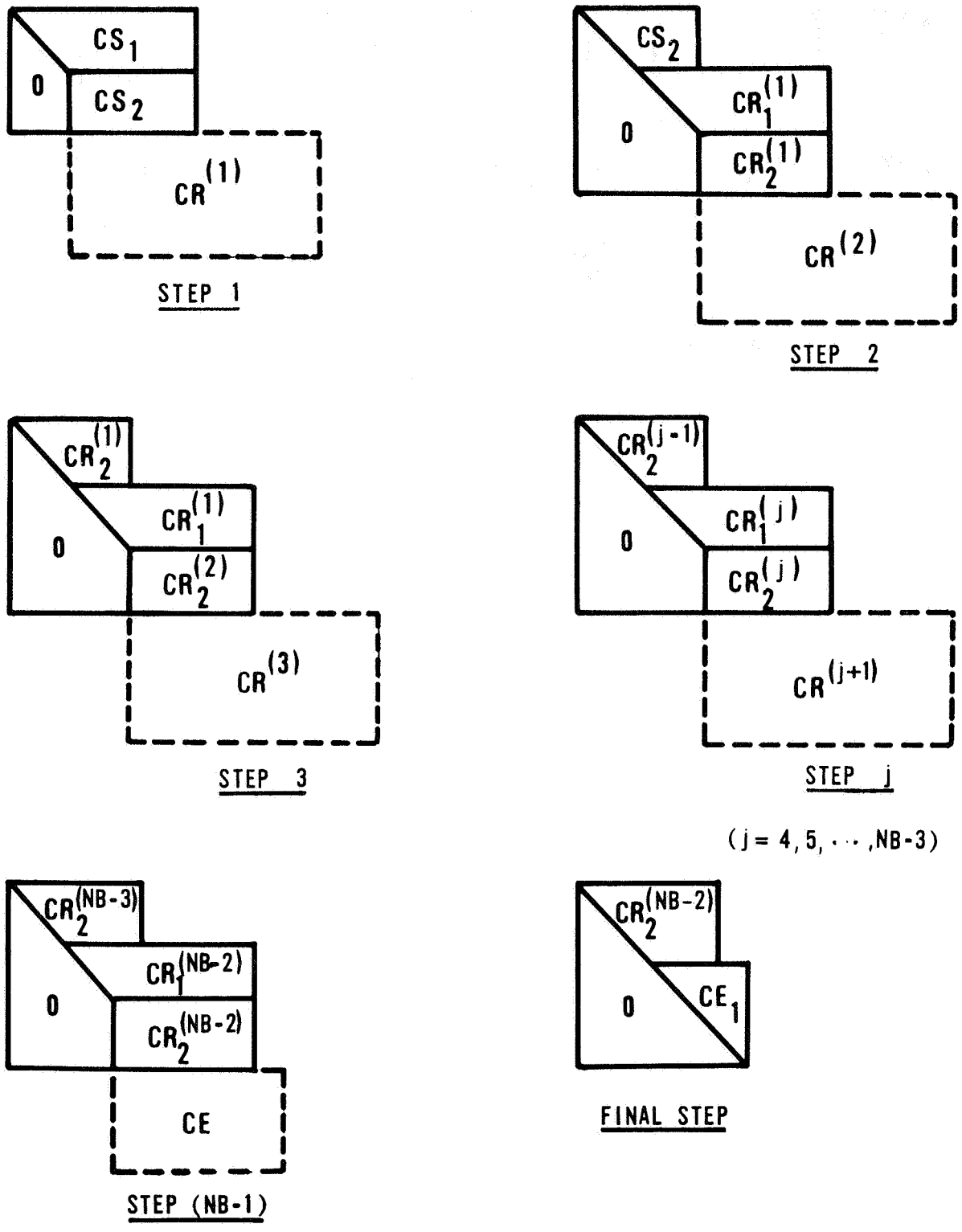

Figure 24.–Elimination Procedure